The IEQ and SAV approaches and their extensions for a class of highly nonlinear gradient flow systems

Jie Shen and Xiaofeng Yang

ABSTRACT. The invariant energy quadratization (IEQ) and scalar auxiliary variable (SAV) approaches are two recently proposed methods to develop linear and unconditionally energy stable schemes for a class of dissipative/conservative systems. The essential idea of these two methods is the energy quadratization strategy, where either the nonlinear potential or its integral is transformed into quadratic forms of the new auxiliary variables. We present the IEQ and SAV approaches in a unified and more general setting, show a few typical applications to problems with moderately stiff nonlinearities, and then present the stabilized IEQ and SAV approaches to deal with several complex systems with highly stiff nonlinear terms.

1. Introduction

The ability of fast and accurate simulation of complex phenomena governed by highly complex nonlinear systems is central to our understanding of many important issues in emerging research fields, such as advanced materials, quantum mechanics, semiconductors, optimal transport, non-convex optimization, etc. Mathematically, these nonlinear systems often take the form of gradient flows or conservative systems. However, it is very challenging to develop accurate and energy stable schemes for these highly complex nonlinear systems. Simple fully-implicit or explicit type approaches to discretize the nonlinear terms will induce severe stability conditions on time steps, so they are not efficient in practice. Many efforts had been devoted to develop unconditionally energy stable schemes without any time step constraints, for instance, the fully implicit methods [**15**, **20**], convex splitting approach [**1**, **18**, **19**, **33**, **45**], the linear stabilization approach [**29**, **37**, **38**, **47**, **65**], the IEQ method [**49**, **50**, **55**, **58**, **63**], the SAV method (cf. [**10**, **35**, **36**]), and a variety of other type methods, see [**21**, **22**, **26**, **32**], etc. We refer to a recent review paper, [**14**] and the references therein, for a detailed account on these efforts.

The IEQ and SAV approaches, which are developed very recently, overcome typical challenges and provide great flexibilities to treat complicated nonlinear terms. Thanks to their simplicity, efficiency, and generality, these two approaches can be applied to a large class of problems with energy dissipation/conservation. In the last couple of years, the IEQ and SAV approaches have been successfully applied to, for instances, the diblock copolymer model [**12**, **49**], the molecular beam epitaxial thin-film model [**11**, **57**], the three components phase-field model in [**58**], the phase-field surfactant model in [**46**, **52**, **53**], the phase-field vesicle membrane model in [**10**, **52**], the phase-field model for moving contact lines in [**54**], the incompressible Navier-Stokes equations in [**31**], the multi-component two-phase flow in [**28**], the strongly anisotropic Cahn-Hilliard model in [**7**, **48**], the solidification phase-field model with/without melt convection in [**6**, **50**], the one- and multi-component BECs in [**9**], the Sine-Gordon equations in [**25**], and the nonlocal Cahn-Hilliard Equation in [**56**], etc.

In this note, we introduce the IEQ and SAV approaches in a unified framework with a more general setting. Then, we present a few typical applications of the IEQ and SAV approaches to several problems with moderately stiff nonlinearities for which the IEQ and SAV approaches can be directly applied successfully. However, complex systems with highly stiff nonlinear terms, direct application of the IEQ and SAV approaches will need exceedingly small time steps to achieve reasonable accuracy. For this type of problems, we need to combine the IEQ and SAV approaches with proper stabilizations. We show that the stabilized IEQ and SAV approaches are very effective to deal with complex systems with highly stiff nonlinear terms such as the anisotropic Cahn-Hilliard model, the anisotropic dendritic model, the phase-field crystal model with a large vacancy potential, etc.

The rest of the paper is organized as follows. In Section 2, we present the IEQ and SAV approaches in a unified framework with a general setting. In Section 3, we apply these two approaches to several gradient flows with moderate nonlinearities, including the phase-field crystal model, the molecular beam epitaxial model, the three-component phase-field model. In Section 4, we introduce the stabilized IEQ and SAV approaches to deal with several applications with highly stiff nonlinear terms, including the anisotropic Cahn-Hilliard model, the anisotropic dendritic model, the phase-field crystal model with a large vacancy potential, and present ample numerical results to show that the stabilization is essential for these highly stiff problems. We conclude with some remarks in Section 5.

2. The IEQ and SAV approaches

We consider the following Lyapunov energy functional,

$$(2.1) \qquad E(\phi) = \int_{\Omega} (\frac{1}{2}\phi \mathcal{L}\phi + F(\phi))d\boldsymbol{x},$$

where $\phi(\boldsymbol{x}, t)$ is the unknown function, $\boldsymbol{x} \in \Omega \subseteq \mathbb{R}^d$ ($d = 2, 3$), $\mathcal{L}$ is a linear self-adjoint positive definite operator, and $F(\phi)$ is the nonlinear part of the total free energy. For instance, in the commonly used phase-field models, $\phi \mathcal{L}(\phi) = |\nabla \phi|^2$ and $F(\phi) = \frac{1}{4\epsilon^2}(\phi^2 - 1)^2$ with $\epsilon \ll 1$ that causes *stiffness*.

To fix the idea, we consider a general gradient flow that reads as:

$$(2.2) \qquad\qquad \phi_t = -\mathcal{G}\mu,$$

$$(2.3) \qquad\qquad \mu = \frac{\delta E}{\delta \phi} = \mathcal{L}\phi + f(\phi),$$

subject to the periodic boundary condition or homogeneous Neumann condition for ϕ and μ and initial condition $\phi|_{t=0} = \phi_0$. In the above, $\mathcal{G}$ is a positive definite operator describing the relaxation process of the gradient flow, for instances, $\mathcal{G} = I$ for L^2-gradient flow, or $\mathcal{G} = -\Delta$ for H^{-1}-gradient flow, μ is the chemical potential, $f(\phi) = F'(\phi)$. By taking the L^2-inner products of (2.2) with μ and of (2.3) with ϕ_t, we obtain the energy law for the above system

$$\frac{d}{dt}E(\phi) = -(\mathcal{G}\mu, \mu) \le 0.$$

2.1. IEQ approach. We now present the so-called IEQ approach [**49**, **50**, **55**, **58**, **63**].

We assume the nonlinear potential $F(\phi)$ *is bounded from below*, i.e.,

$$F(\phi) > -C_0,$$

for some $C_0 > 0$, and introduce a new variable $U(\phi)$ through the following *quadratization* formula, that is

$$U(\phi) = \sqrt{F(\phi) + C_0}.$$

Thus the total energy in terms of ϕ and U turns to

$$(2.4) \qquad\qquad E(\phi, U) = \int_\Omega \Big(\frac{1}{2}\phi\mathcal{L}\phi + U^2\Big)d\boldsymbol{x} - C_0|\Omega|.$$

We denote $H(\phi) = 2\frac{d}{d\phi}U(\phi) = \frac{f(\phi)}{\sqrt{F(\phi)+C_0}}$, then the system (2.2)-(2.3) can be rewritten as:

$$(2.5) \qquad\qquad \phi_t = -\mathcal{G}\mu,$$

$$(2.6) \qquad\qquad \mu = \mathcal{L}\phi + H(\phi)U,$$

$$(2.7) \qquad\qquad U_t = \frac{1}{2}H(\phi)\phi_t,$$

with the initial conditions $\phi|_{t=0} = \phi_0$, $U|_{t=0} = \sqrt{F(\phi_0) + C_0}$. Note (2.7) is actually an ODE for the new variable U, therefore, no boundary conditions is needed for U.

It is rather straightforward to develop efficient linear schemes for the system (2.5)-(2.7) with the principle of treating linear terms implicitly and all nonlinear terms explicitly. For example, a second-order scheme based on the second-order backward difference formula (BDF) is as follows:

Having computed ϕ^n and ϕ^{n-1}, we update ϕ^{n+1} by solving

$$(2.8) \qquad \frac{3\phi^{n+1} - 4\phi^n + \phi^{n-1}}{2\delta t} = -\mathcal{G}\mu^{n+1},$$

$$(2.9) \qquad\qquad \mu^{n+1} = \mathcal{L}\phi^{n+1} + H^{*,n+1}U^{n+1},$$

$$(2.10) \qquad 3U^{n+1} - 4U^n + U^{n-1} = \frac{1}{2}H^{*,n+1}(3\phi^{n+1} - 4\phi^n + \phi^{n-1}),$$

where $H^{*,n+1} = H(\phi^{*,n+1})$ with $\phi^{*,n+1} = 2\phi^n - \phi^{n-1}$.

It is clear that the above scheme is second-order accurate. Furthermore, taking the L^2 inner products of (2.8) with $-2\delta t\mu^{n+1}$, of (2.9) with $3\phi^{n+1} - 4\phi^n + \phi^{n-1}$,

and of (2.10) with $-2U^{n+1}$, respectively, summing up the results and noticing that the two terms with $H^{*,n+1}$ cancel each other regardless the form of $H(\phi)$, we obtain immediately the following result:

THEOREM 2.1. *The scheme* (2.8)-(2.10) *is unconditionally energy stable in the sense that*

$$\bar{E}_1^{n+1} - \bar{E}_1^n = - \delta t(\mathcal{G}\mu^{n+1}, \mu^{n+1})$$
$$- \int_\Omega \frac{1}{4}(\phi^{n+1} - 2\phi^n + \phi^{n-1})\mathcal{L}(\phi^{n+1} - 2\phi^n + \phi^{n-1})d\boldsymbol{x}$$
$$+ \int_\Omega \frac{1}{2}(U^{n+1} - 2U^n + U^{n-1})^2 d\boldsymbol{x},$$

where

$$\bar{E}_1^{n+1} = \int_\Omega \left(\frac{1}{2}(U^{n+1})^2 + \frac{1}{2}(2U^{n+1} - U^n)^2 + \frac{1}{4}\phi^{n+1}\mathcal{L}\phi^{n+1} \right) d\boldsymbol{x}$$
$$+ \int_\Omega \frac{1}{4}(2\phi^{n+1} - \phi^n)\mathcal{L}(2\phi^{n+1} - \phi^n)d\boldsymbol{x}.$$

Note that the system (2.8)-(2.10) is linear but coupled in (ϕ, μ, U). However, instead of solving the coupled system (2.8)-(2.10) directly, we can eliminate U as follows. Note the nonlinear coefficient H of the new variable U is treated explicitly in (2.9), thus we can rewrite it as

$$(2.11) \qquad\qquad U^{n+1} = \frac{1}{2}H^{*,n+1}\phi^{n+1} + g_1^n,$$

where g_1^n includes all explicit terms. Using this equality, (2.9)-(2.10) can be rewritten as

$$(2.12) \qquad\qquad \frac{3}{2\delta t}\phi^{n+1} + \mathcal{G}\mu^{n+1} = \frac{4\phi^n - \phi^{n-1}}{2\delta t},$$
$$(2.13) \qquad\qquad -\mu^{n+1} + P(\phi^{n+1}) = \tilde{g}_1^n,$$

where $\tilde{g}_1^n$ includes all explicit terms, $P(\phi)$ is a linear and symmetric positive definite operator that is defined as

$$P(\phi) = \mathcal{L}\phi + \frac{1}{2}H^{*,n+1}H^{*,n+1}\phi.$$

Therefore, in practice one can solve ϕ^{n+1} and μ^{n+1} directly from (2.12)-(2.13). Once ϕ^{n+1} is obtained, U^{n+1} is automatically given by (2.11). The well-posedness of the linear system (2.12)-(2.13) then follows directly from the Lax-Milgram Theorem [**48**, **54**, **58**].

The operator $P(\phi)$ in the scheme (2.13) includes a variable-coefficient $\frac{1}{2}H^nH^n$ for the term ϕ^{n+1}. Explicitly building those time-dependent matrices are usually expensive. So in practice, an efficient way is to use a preconditioned conjugate gradient type solver which does not require building the system matrix explicitly. An efficient time-independent preconditioner is to replace the variable coefficient $\frac{1}{2}H^nH^n\phi^{n+1}$ by a suitable constant coefficient.

2.2. SAV approach. The SAV approach [**10**, **35**, **36**] is inspired by the IEQ approach, but with extended applicability and more efficient implementation. Given a free energy in the form of (2.1), we assume $\int_\Omega F(\phi)d\boldsymbol{x}$ is bounded from below, i.e.,

$$\int_\Omega F(\phi)d\boldsymbol{x} > -C_0$$

for some $C_0 > 0$, and introduce a new auxiliary scalar variable $u(\phi)$ through the following *quadratization* formula:

$$(2.14) \qquad u(\phi) = \sqrt{\int_\Omega F(\phi)d\boldsymbol{x} + C_0}.$$

Denoting $K(\phi) = \dfrac{f(\phi)}{\sqrt{\int_\Omega F(\phi)d\boldsymbol{x}+C_0}}$, the system (2.2)-(2.3) can be rewritten as:

$$(2.15) \qquad\qquad \phi_t = -\mathcal{G}\mu,$$

$$(2.16) \qquad\qquad \mu = \mathcal{L}\phi + K(\phi)u,$$

$$(2.17) \qquad\qquad u_t = \frac{1}{2}\int_\Omega K(\phi)\phi_t d\boldsymbol{x},$$

with the initial conditions $\phi|_{t=0} = \phi_0, \ u|_{t=0} = \sqrt{\int_\Omega F(\phi_0)d\boldsymbol{x} + C_0}$.

Then, a second-order linear scheme based on BDF2 for the above reformulated system can be constructed as follows:

Having computed ϕ^n and ϕ^{n-1}, we update ϕ^{n+1} by solving

$$(2.18) \qquad \frac{3\phi^{n+1} - 4\phi^n + \phi^{n-1}}{2\delta t} = -\mathcal{G}\mu^{n+1},$$

$$(2.19) \qquad\qquad \mu^{n+1} = \mathcal{L}\phi^{n+1} + K^{*,n+1}u^{n+1},$$

$$(2.20) \qquad 3u^{n+1} - 4u^n + u^{n-1} = \frac{1}{2}\int_\Omega K^{*,n+1}(3\phi^{n+1} - 4\phi^n + \phi^{n-1})d\boldsymbol{x},$$

where $\phi^{*,n+1} = 2\phi^n - \phi^{n-1}$ and $K^{*,n+1} = K(\phi^{*,n+1})$.

Similar to Theorem 2.1, we can derive the following result.

THEOREM 2.2. *The scheme* (2.18)-(2.20) *is unconditionally energy stable in the sense that*

$$\bar{E}_2^{n+1} - \bar{E}_2^n = - \delta t(\mathcal{G}\mu^{n+1}, \mu^{n+1})$$
$$- \int_\Omega \left(\frac{1}{4}(\phi^{n+1} - 2\phi^n + \phi^{n-1})\mathcal{L}(\phi^{n+1} - 2\phi^n + \phi^{n-1})\right)d\boldsymbol{x}$$
$$- \frac{1}{2}(u^{n+1} - 2u^n + u^{n-1})^2,$$

where

$$\bar{E}_2^{n+1} = \frac{1}{2}(u^{n+1})^2 + \frac{1}{2}(2u^{n+1} - u^n)^2$$
$$+ \int_\Omega \left(\frac{1}{4}\phi^{n+1}\mathcal{L}\phi^{n+1} + \frac{1}{4}(2\phi^{n+1} - \phi^n)\mathcal{L}(2\phi^{n+1} - \phi^n)\right)d\boldsymbol{x}.$$

The main advantage of the SAV scheme is that it can be solved more efficiently. Indeed, the above scheme is only coupled by a scalar u^{n+1} which can be eliminated as follows.

We rewrite (2.20) as

$$(2.21) \qquad u^{n+1} = \frac{1}{2} \int_{\Omega} K^{*,n+1} \phi^{n+1} d\boldsymbol{x} + g_2^n,$$

where g_2^n includes all explicit terms. Using this equality, (2.18)-(2.19) can be rewritten as

$$(2.22) \qquad \mathscr{P}(\phi^{n+1}) + \frac{1}{2}\mathcal{G}K^{*,n+1} \int_{\Omega} K^{*,n+1} \phi^{n+1} d\boldsymbol{x} = \tilde{g}_2^n,$$

where $\tilde{g}_2^n$ includes all explicit terms, and $\mathscr{P}(\cdot)$ is the linear operator that is defined as

$$(2.23) \qquad \mathscr{P}(\psi) = (\frac{3}{2\delta t} + \mathcal{G}L)\psi.$$

Define a linear operator $\mathscr{P}^{-1}(\cdot)$, such that for any function $\phi \in L^2(\Omega)$, $\psi = \mathscr{P}^{-1}(\phi)$ is the solution of the following linear system

$$(2.24) \qquad \mathscr{P}(\psi) = \phi$$

with the periodic or homogeneous Neumann boundary conditions. By applying the operator $\mathscr{P}^{-1}$ to (2.22), then we obtain

$$(2.25) \qquad \phi^{n+1} + \frac{1}{2}\mathscr{P}^{-1}(\mathcal{G}K^{*,n+1}) \int_{\Omega} K^{*,n+1}\phi^{n+1} d\boldsymbol{x} = \mathscr{P}^{-1}(\tilde{g}_2^n).$$

By taking the L^2 inner product of (2.25) with $K^{*,n+1}$, we obtain

$$(2.26) \qquad \int_{\Omega} K^{*,n+1}\phi^{n+1} d\boldsymbol{x} = \frac{\int_{\Omega} K^{*,n+1}\mathscr{P}^{-1}(\tilde{g}_2^n)d\boldsymbol{x}}{1 + \frac{1}{2}\int_{\Omega} K^{*,n+1}\mathscr{P}^{-1}(\mathcal{G}K^{*,n+1})d\boldsymbol{x}}.$$

It is easy to check the term in the denominator $\int_{\Omega} K^{*,n+1}\mathscr{P}^{-1}(\mathcal{G}K^{*,n+1})d\boldsymbol{x} \geq 0$ since $\mathscr{P}^{-1}(\mathcal{G})$ is a positive definite operator.

Furthermore, (2.26) actually provides an explicit formulation for the nonlocal term $\int_{\Omega} K^{*,n+1}\phi^{n+1}d\boldsymbol{x}$. Therefore, in computations, we first find $\psi_1 = \mathscr{P}^{-1}(\tilde{g}_2^n)$ and $\psi_2 = \mathscr{P}^{-1}(\mathcal{G}K^{*,n+1})$, that means to solve the following two linear equations,

$$(2.27) \qquad (\frac{3}{2\delta t} + \mathcal{G}L)\psi_1 = \tilde{g}_2^n,$$

and

$$(2.28) \qquad (\frac{3}{2\delta t} + \mathcal{G}L)\psi_2 = \mathcal{G}K^{*,n+1},$$

with the periodic or homogeneous Neumann boundary conditions. Then, we can obtain ϕ^{n+1} from (2.25) directly.

To summarize, the scheme (2.18)-(2.20) can be easily implemented in the following manner:

- Compute ψ_1 and ψ_2 by solving two linear equations with constant coefficients, (2.27) and (2.28);
- Compute $\int_{\Omega} K^{*,n+1}\phi^{n+1}$ from (2.26) and update u^{n+1} from (2.21);
- Update ϕ^{n+1} from (2.25).

Hence, the total cost at each time step is essentially *solving two linear equations with constant coefficients*. Hence, this scheme is extremely efficient and easy to implement.

2.3. Some remarks. The main difference between the IEQ approach and the SAV approach is that the auxiliary function in the IEQ approach is space-time dependent while in the SAV approach is only time-dependent. The consequence of this difference is that in the IEQ approach, one has to solve a linear system with time dependent variable coefficients, while in the SAV approach, one only needs to solve a linear system with constant coefficients which can be solved very efficiently by fast elliptic solvers. Moreover, even for problems with multiple components, the SAV approach leads to a sequence of decoupled linear systems with constant coefficients. On the other hand, the IEQ approach offers stronger coupling which can be advantageous in certain situations such as problems with local constraints, such an example is provided in [**25**] where the IEQ approach applied to the sine-Gordon equation not only conserves the global energy but also enforce a local energy law.

We described the IEQ/SAV approaches using a second-order BDF2 method as an example. One can also use other types of linear schemes. For example, a second-order IEQ scheme based on the Crank-Nicolson for (2.5)-(2.7) is:

Having computed ϕ^n and ϕ^{n-1}, we update ϕ^{n+1} by solving

$$(2.29) \qquad \frac{\phi^{n+1} - \phi^n}{\delta t} = -\mathcal{G}\mu^{n+\frac{1}{2}},$$

$$(2.30) \qquad \mu^{n+\frac{1}{2}} = \mathcal{L}\frac{\phi^{n+1} + \phi^n}{2} + H^{*,n+\frac{1}{2}}\frac{U^{n+1} + U^n}{2},$$

$$(2.31) \qquad U^{n+1} - U^n = \frac{1}{2}H^{*,n+\frac{1}{2}}(\phi^{n+1} - \phi^n),$$

where $H^{*,n+\frac{1}{2}} = H(\phi^{*,n+\frac{1}{2}})$ with $\phi^{*,n+\frac{1}{2}} = \frac{3}{2}\phi^n - \frac{1}{2}\phi^{n-1}$. We can easily show that the above scheme is unconditionally energy stable in the sense that

$$\hat{E}_1^{n+1} - \hat{E}_1^n = -\delta t(\mathcal{G}\mu^{n+\frac{1}{2}}, \mu^{n+\frac{1}{2}}),$$

where

$$\hat{E}_1^{n+1} = \int_\Omega ((U^{n+1})^2 + \frac{1}{2}\phi^{n+1}\mathcal{L}\phi^{n+1})d\boldsymbol{x}.$$

Similarly, we can construct kth-order schemes with BDF-k ($3 \le k \le 6$) formula in the IEQ/SAV approach. While we can not prove rigorously that these high-order BDF schemes are unconditionally energy stable, numerical results indicate that they do achieve expected order of accuracy and enjoy excellent stability [**36**].

We observe that the SAV scheme based on Crank-Nicolson does not introduce any additional dissipation so it preserves the energy if $\mathcal{G}$ is skew-symmetric or energy dissipation rate if $\mathcal{G}$ is positive definite. In general, the SAV scheme based on Crank-Nicolson is preferred for conservative systems while the SAV scheme based on BDF formulae should be used for dissipative systems.

While, for the sake of simplicity, we described the IEQ/SAV schemes in semi-discrete form, the above stability results carry over to any consistent Galerkin type approximations, e.g. finite- elements or spectral methods, as well as finite-difference method with proper summation-by-parts.

While the splitting of the free energy in (2.1) can be arbitrary, it is essential, for the sake of accuracy, to have a splitting with a "dominating" operator $\mathcal{L}$. Otherwise, exceedingly small time steps may be needed to obtain accurate results. Sometimes, the obvious splitting, e.g, $E(\phi) = \int_\Omega(\frac{1}{2}|\nabla\phi|^2 + \frac{1}{4\epsilon^2}(\phi^2 - 1)^2)d\boldsymbol{x}$ with $\epsilon \ll 1$, may

not be suitable. We refer to Section 3.1 in [**36**] for such an example and a strategy to deal with it.

To take the full advantages of the unconditional energy stability, the IEQ/SAV schemes should be coupled with an adaptive time-stepping scheme so that the time step is determined by accuracy requirement only without worrying about stability. We refer to Section 4.2 in [**36**] for some details in this regards.

Thanks to the unconditional energy stability, one can show that the convergences of IEQ/SAV methods and establish corresponding error estimates without assuming the uniform Lipschitz condition on $f(\phi)$. We refer to [**34**, **55**] for the convergence and error estimates of IEQ/SAV methods in the semi-discrete case for the Allen-Cahn and Cahn-Hilliard equations, to [**30**] for error estimates of the SAV methods with finite-differences and to [**66**] for error estimates of the SAV methods with finite-elements, to [**25**] for error analysis of an IEQ method with finite-difference for the sine-Gordon equation.

3. Applications of IEQ/SAV approaches to problems with moderately stiff nonlinear terms

In this section, we consider several models with low or moderate stiff nonlinear terms so that the IEQ/SAV approaches can be directly applied successfully.

3.1. Phase-field crystal model. In [**16**, **17**, **44**], the authors considered a very simple phase-field crystal (PFC) model that showed great versatility to study the dynamics of atomic-scale crystal growth on diffusive time scales. A phase-field variable that represents the concentration field of a coarse-grained temporal average of the density of atoms, is introduced to describe the phase transition from the liquid phase to the crystal phase. Thus, to generate the periodic structure of a crystal lattice, by incorporating a specific form of the spatial gradients in the free energy is postulated, the model is flexible and can be applied to simulate various phenomena, for instances, epitaxial growth, material hardness, grain growth, reconstructive phase transitions, and crack propagations.

The PFC model is described by the following total free energy

$$(3.1) \qquad E(\phi) = \int_\Omega \Big(\frac{\phi}{2} \mathcal{L}_1^2 (\mathcal{L}_2^2 + r^2)\phi + F(\phi) \Big) d\boldsymbol{x},$$

where $\mathcal{L}_1 = \Delta + I$ and $\mathcal{L}_2 = \Delta + q^2$ with Δ being the Laplace operator, $F(\phi) = \frac{1}{4}\phi^4 - \frac{\eta}{2}\phi^2$ is the nonlinear smoothing potential, and r, q, η are three positive constants.

By taking the variational derivative of the total free energy (3.1) in H^{-1}, we obtain the PDE system as

$$(3.2) \qquad \phi_t = M\Delta\mu,$$

$$(3.3) \qquad \mu = \frac{\delta E}{\delta \phi} = \mathcal{L}_1^2(\mathcal{L}_2^2 + r^2)\phi + f(\phi).$$

Note that free energy in (3.1) is already in the form of (2.1) so that both IEQ and SAV approaches can be directly applied. We consider, for example, the IEQ approach. Let $U = \sqrt{F(\phi) + C_0}$ so the equivalent system reads as

$$(3.4) \qquad \phi_t = M\Delta\mu,$$

$$(3.5) \qquad \mu = \mathcal{L}_1^2(\mathcal{L}_2^2 + r^2)\phi + HU,$$

$$(3.6) \qquad U_t = \frac{1}{2}H\phi_t,$$
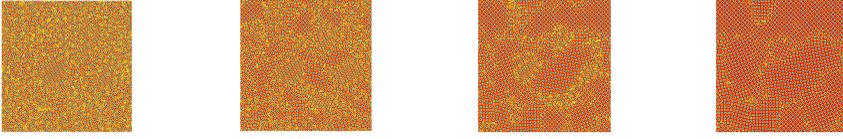
(a) The formation of the FCC pattern structure.
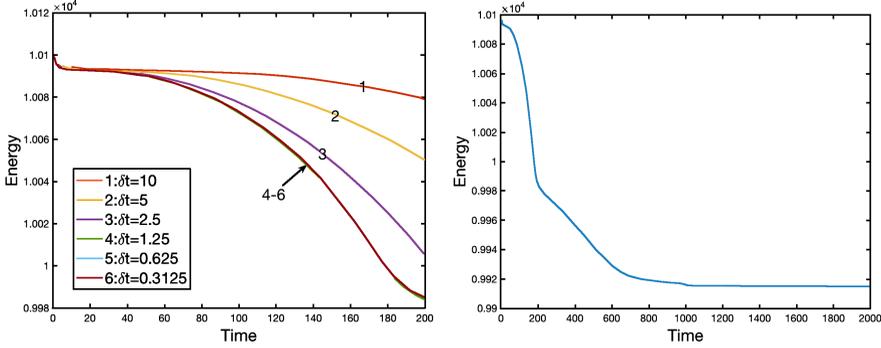
(b) Time evolution of the total free energy functional computed by using different time steps.

(c) Time evolution of the total free energy by using $\delta t = 0.1$.

FIGURE 3.1. (a) The formation of FCC pattern through the simulation of the phase separation with the initial average density $\bar{\phi} = 0.23$ and parameter $\eta = 0.195$. Snapshots of the numerical approximation of ϕ are taken at $t = 20, 100, 300$, and 800. (b) Time evolution of the total free energy functional computed by using nine different time steps. (c) Time evolution of the free energy functional by using $\delta t = 0.1$.

where $H = \dfrac{f(\phi)}{\sqrt{F(\phi) + C_0}}$.

Based on the second-order Adam-bashforth time stepping scheme, a second-order scheme can be constructed as follows:

Having computed ϕ^n and ϕ^{n-1}, we update ϕ^{n+1} by solving

$$(3.7) \qquad \frac{3\phi^{n+1} - 4\phi^n + \phi^{n-1}}{2\delta t} = \Delta\mu^{n+1},$$

$$(3.8) \qquad \mu^{n+1} = \mathcal{L}_1^2(\mathcal{L}_2^2 + r^2)\phi^{n+1} + H^{*,n+1}U^{n+1},$$

$$(3.9) \qquad 3U^{n+1} - 4U^n + U^{n-1} = \frac{1}{2}H^{*,n+1}(3\phi^{n+1} - 4\phi^n + \phi^{n-1}),$$

where $\phi^{*,n+1} = 2\phi^n - \phi^{n-1}$ and $H^{*,n+1} = H(\phi^{*,n+1})$. The above scheme has been implemented in [51, 61] to study the phase transition behaviors of the PFC model. We present below some numerical simulations with model parameters $M = 1, q = \sqrt{2}, r = 0, \eta = 0.195$. The computational domain is set as $[0, 256]^2$, and the initial condition is $\phi_0 = 0.23(1 + \text{rand}(x, y))$. We discretize the space by using 513^2 Fourier modes. Snapshots of the phase-field variable ϕ are shown in Fig. 3.1(a). We observe that the crystals transform to the face-centered-cubic (FCC) structure from the spontaneous lattice structure. In Fig. 3.1(b), we plot the time evolution of the total free energy for nine different time step sizes until $t = 200$. All energy curves
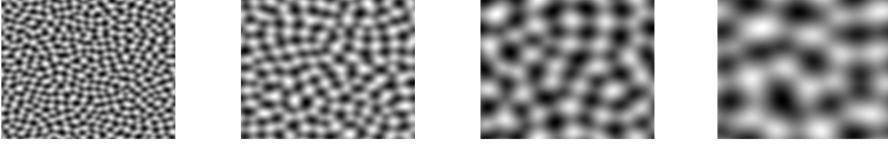
FIGURE 3.2. The isolines of the numerical solutions of the height function ϕ for the epitaxial thin film model without slope selection with the random initial condition. Snapshots are taken at $t = 1, 10, 100, 500$.

decay monotonically for all time step sizes, which confirms that the algorithm is unconditionally energy stable. In Fig. 3.1(c), we show the time evolution of the free energy functional by using the time step $\delta t = 0.1$.

3.2. Molecular beam epitaxial model. The continuum model for the molecular beam epitaxial model is a powerful tool to understand the mechanisms of thin film growth, where epitaxy is referred to the deposition of a crystalline overlayer on a substrate.

Let $\phi(x)$ be a height function, the total phenomenological free energy for the epitaxial thin film model is as follows,

$$(3.10) \qquad E(\phi) = \int_{\Omega} \left(\frac{\epsilon^2}{2} (\Delta\phi)^2 + F(\nabla\phi) \right) d\boldsymbol{x}$$

where the nonlinear potential is either Ginzburg-Landau double well potential (with slope selection) $F(\nabla\phi) = (1 - |\nabla\phi|^2)^2$ or a nonlinear logarithmic potential (without slope selection) $F(\nabla\phi) = -\frac{1}{2}\ln(1 + |\nabla\phi|^2)$.

For the slope selection case, the IEQ method can be applied since the nonlinear potential is bounded from below, see [**57**]. But for the model without slope selection, the logarithmic nonlinear potential is not bounded from below, so the IEQ method can not be applied directly. However, with a proper splitting of the free energy, we can apply the SAV method. The details are given below.

Note that for any $\epsilon > 0$, there exists a constant $c > 0$ such that the following property holds (cf. [**11**]),

$$\int_{\Omega} \left(\frac{\epsilon^2}{4} |\Delta\phi|^2 - \frac{1}{2}\ln(1 + |\nabla\phi|^2) \right) d\boldsymbol{x} \geq c_0,$$

where $c_0 = \frac{1}{2}(\ln(\frac{\epsilon^2}{2c^2}) - \frac{\epsilon^2}{2c^2} + 1)|\Omega|$. Hence, we can split the free energy as follows:

$$E(\phi) = \int_{\Omega} \left\{ \frac{\epsilon^2}{4} (\Delta\phi)^2 + \left(\frac{\epsilon^2}{4} |\Delta\phi|^2 - \frac{1}{2}\ln(1 + |\nabla\phi|^2) \right) \right\} d\boldsymbol{x},$$

and define a SAV by

$$(3.11) \qquad u(t) = \sqrt{\int_{\Omega} \left(\frac{\epsilon^2}{4} |\Delta\phi|^2 - \frac{1}{2}\ln(1 + |\nabla\phi|^2) \right) d\boldsymbol{x} + C_0},$$

where C_0 is a positive constant to ensure the radicands are positive. For example, we can choose $C_0 = -c_0 + 1$. Thus the equivalent SAV system reads as

$$\phi_t + M(\frac{\epsilon^2}{2}\Delta^2\phi + K(\phi)u) = 0,$$

$$u_t = \frac{1}{2}\int_\Omega K(\phi)\phi_t d\boldsymbol{x},$$

where M is a mobility function, and

$$K(\phi) = \frac{\frac{\epsilon^2}{2}\Delta^2\phi + \nabla\cdot(\frac{\nabla\phi}{1+|\nabla\phi|^2})}{\sqrt{\int_\Omega(\frac{\epsilon^2}{4}|\Delta\phi|^2 - \frac{1}{2}\ln(1+|\nabla\phi|^2))d\boldsymbol{x} + C_0}}.$$

Then a second-order BDF2 scheme for the above system reads as follows,

$$(3.12) \quad \frac{3\phi^{n+1} - 4\phi^n + \phi^{n-1}}{2\delta t} \quad + \quad M(\epsilon^2\Delta^2\phi^{n+1} + K^{*,n+1}u^{n+1}) = 0,$$

$$(3.13) \quad 3u^{n+1} - 4u^n + u^{n-1} \quad = \quad \frac{1}{2}\int_\Omega K^{*,n+1}(3\phi^{n+1} - 4\phi^n + \phi^{n-1})d\boldsymbol{x},$$

where $\phi^{*,n+1} = 2\phi^n - \phi^{n-1}$ and $K^{*,n+1} = K(\phi^{*,n+1})$.

To validate the above numerical scheme, we simulated the coarsening dynamics in [11] by choosing a random initial condition varying from -0.001 to 0.001. The parameters are $\epsilon = 0.03$, $M = 1$. The computational domain is $\Omega = [0, 12.8]^2$, and we use 513×513 Fourier modes in space. In [11], various numerical results confirming unconditional energy stability are presented. As an example, we show in Fig. 3.2 snapshots of numerical solutions of the height function ϕ at various times.

3.3. Three-component Cahn-Hilliard model. We consider a three-component Cahn-Hilliard phase-field model presented in [2, 3]. This model was derived by adopting three independent phase-field variables, and postulating the nonlinear part of the total phenomenological free energy to be a summation of the double-well potentials for each phase. To ensure a hyperplane link condition for the three phase variables at each point, a Lagrange multiplier term is added into the system. More precisely, assuming a system consists of three material components, we introduce ϕ_i ($i = 1, 2, 3$) to describe the volume fraction of the i-th phase such that the following hyperplane link condition is satisfied

$$(3.14) \qquad \phi_1 + \phi_2 + \phi_3 = 1.$$

The total free energy for the three-phase system is postulated as:

$$(3.15) \quad E(\phi_1, \phi_2, \phi_3) = \frac{3}{8}\epsilon\sum_{i=1}^{3}\int_\Omega \Sigma_i|\nabla\phi_i|^2 d\boldsymbol{x} + \frac{12}{\epsilon}\int_\Omega F(\phi_1, \phi_2, \phi_3)d\boldsymbol{x},$$

in which, the nonlinear potential $F(\phi_1, \phi_2, \phi_3)$ reads as:

$$F(\phi_1, \phi_2, \phi_3) = \frac{\Sigma_1}{2}\phi_1^2(1-\phi_1)^2 + \frac{\Sigma_2}{2}\phi_2^2(1-\phi_2)^2 + \frac{\Sigma_3}{2}\phi_3^2(1-\phi_3)^2 + 3\Lambda\phi_1^2\phi_2^2\phi_3^2,$$

where Λ is a non-negative constant, ϵ is related to the interfacial width, the coefficients of entropic terms Σ_i (note Σ_i might be negative) are determined by the surface tension parameters $\sigma_{12}, \sigma_{13}, \sigma_{23}$, i.e.,

$$\Sigma_1 = \sigma_{12} + \sigma_{13} - \sigma_{23}, \ \Sigma_2 = \sigma_{12} + \sigma_{23} - \sigma_{13}, \ \Sigma_3 = \sigma_{13} + \sigma_{23} - \sigma_{12}.$$

Then the three-component Cahn-Hilliard system that we consider is the H^{-1} gradient flow of the above free energy:

$$(3.16) \qquad \phi_{it} = M\Delta\frac{\mu_i}{\Sigma_i},$$

$$(3.17) \qquad \mu_i = -\frac{3}{4}\epsilon\Sigma_i\Delta\phi_i + \frac{12}{\epsilon}(f_i + \beta), \ i = 1, 2, 3,$$

where M is the mobility constant, $f_i = \frac{\delta F(\phi_1, \phi_2, \phi_3)}{\delta\phi_i}$, and β is a Lagrange multiplier to ensure the hyperplane link condition (3.14) which leads to

$$\beta = -\frac{1}{\Sigma_T}(\frac{f_1}{\Sigma_1} + \frac{f_2}{\Sigma_2} + \frac{f_3}{\Sigma_3}) \text{ with } \frac{1}{\Sigma_T} = \frac{1}{\Sigma_1} + \frac{1}{\Sigma_2} + \frac{1}{\Sigma_3}.$$

It can be shown [58, Lemma 2,2] that there exists $C_0 > 0$ such that $\int_\Omega F(\phi_1, \phi_2, \phi_3)d\boldsymbol{x} > -C_0$, we can rewrite the total free energy (3.15) as

$$E(u, \phi_1, \phi_2, \phi_3) = \frac{3}{8}\epsilon\sum_{i=1}^{3}\int_\Omega \Sigma_i|\nabla\phi_i|^2d\boldsymbol{x} + \frac{12}{\epsilon}(u^2 - C_0).$$

Thus we can apply IEQ and SAV approaches directly.

In [58], the IEQ method is applied to solve the above system. Below we shall adapt the SAV approach and define

$$u(t) = \sqrt{\int_\Omega F(\phi_1, \phi_2, \phi_3)d\boldsymbol{x} + C_0}.$$

Then, the system (3.16) can be rewritten as

$$(3.18) \qquad \phi_{it} = \frac{M}{\Sigma_i}\Delta\mu_i,$$

$$(3.19) \qquad \mu_i = -\frac{3}{4}\epsilon\Sigma_i\Delta\phi_i + \frac{12}{\epsilon}(K_i + \alpha)u, \quad i = 1, 2, 3,$$

$$(3.20) \qquad u_t = \frac{1}{2}\sum_{i=1}^{3}\int_\Omega K_i\phi_{it}d\boldsymbol{x},$$

where

$$K_i = \frac{f_i}{\sqrt{\int_\Omega F(\phi_1, \phi_2, \phi_3)d\boldsymbol{x} + C_0}}, \ \alpha = -\frac{1}{\Sigma_T}(\frac{K_1}{\Sigma_1} + \frac{K_2}{\Sigma_2} + \frac{K_3}{\Sigma_3}).$$

A second-order SAV-BDF2 scheme for the above system is as follows.

Assuming $(\phi_1, \phi_2, \phi_3, u)^n$ and $(\phi_1, \phi_2, \phi_3, u)^{n-1}$ are known, we update $(\phi_1, \phi_2, \phi_3, u)^{n+1}$ by the following:

$$(3.21) \qquad \frac{3\phi_i^{n+1} - 4\phi_i^n + \phi_i^{n-1}}{2\delta t} = M\Delta\frac{\mu_i^{n+1}}{\Sigma_i},$$

$$(3.22) \qquad \mu_i^{n+1} = -\frac{3}{4}\epsilon\Sigma_i\Delta\phi_i^{n+1} + \frac{12}{\epsilon}(K_i^{*,n+1} + \alpha^{*,n+1})u^{n+1}$$

$$(3.23) \qquad 3u^{n+1} - 4u^n + u^{n-1} = \frac{1}{2}\sum_{i=1}^{3}\int_\Omega H_i^{*,n+1}(3\phi_i^{n+1} - 4\phi_i^n + \phi_i^{n-1})d\boldsymbol{x},$$

for $i = 1, 2, 3$, where

$$\phi_i^{*,n+1} = 2\phi_i^n - \phi_i^{n-1}, K_i^{*,n+1} = K_i(\phi_1^{*,n+1}, \phi_2^{*,n+1}, \phi_3^{*,n+1}),$$

$$\alpha^{*,n+1} = -\frac{1}{\Sigma_T}\left(\frac{K_1^{*,n+1}}{\Sigma_1} + \frac{K_2^{*,n+1}}{\Sigma_2} + \frac{K_3^{*,n+1}}{\Sigma_3}\right).$$

We can easily prove the solutions of the scheme (3.21)-(3.23) satisfies the hyperplane link condition (3.14). Thus one can first solve ϕ_1 and ϕ_2, and then update ϕ_3 by the hyperplane link condition (3.14). By rewriting (3.23) as,

$$u^{n+1} = \frac{1}{2}\int_\Omega T_1\phi_1^{n+1}d\boldsymbol{x} + \frac{1}{2}\int_\Omega T_2\phi_2^{n+1}d\boldsymbol{x} + r^n,$$

where

$$T_1 = \hat{H}_1^{*,n+1} - \hat{H}_3^{*,n+1}, T_2 = \hat{H}_2^{*,n+1} - \hat{H}_3^{*,n+1}, \hat{H}_i^{*,n+1} = H_i^{*,n+1} + \alpha^{*,n+1}, i = 1, 2, 3,$$

and r^n includes all explicit terms. Then we can derive the following system for $(\phi_1^{n+1}, \phi_2^{n+1})$ from (3.21)-(3.22) $(i = 1, 2)$:

$$(3.24) \qquad \mathscr{P}(\phi_1^{n+1}) - \frac{6}{\Sigma_1\epsilon^2}\Delta(\hat{H}_1^{*,n+1})\left(\int_\Omega T_1\phi_1^{n+1}d\boldsymbol{x} + \int_\Omega T_2\phi_2^{n+1}d\boldsymbol{x}\right) = r_1^n,$$

$$(3.25) \qquad \mathscr{P}(\phi_2^{n+1}) - \frac{6}{\Sigma_2\epsilon^2}\Delta(\hat{H}_2^{*,n+1})\left(\int_\Omega T_1\phi_1^{n+1}d\boldsymbol{x} + \int_\Omega T_2\phi_2^{n+1}d\boldsymbol{x}\right) = r_2^n,$$

where the operator $\mathscr{P}$ is defined as

$$\mathscr{P}(\psi) = \frac{3}{2M\epsilon\delta t}\psi + \frac{3}{4}\Delta^2\psi,$$

and r_1^n, r_2^n include all explicit terms.

Define a linear operator $\mathscr{P}^{-1}(\cdot)$, such that for any function $\phi \in L^2(\Omega)$, $\psi = \mathscr{P}^{-1}(\phi)$ is the solution of the following linear system

$$\mathscr{P}(\psi) = \phi,$$

with corresponding boundary conditions, i.e., periodic boundary conditions or homogeneous Neumann boundary condition for ψ and $\Delta\psi$. By applying the operator $\mathscr{P}^{-1}$ to (3.24) and (3.25), we obtain

$$(3.26)\quad \phi_1^{n+1} - \frac{6}{\Sigma_1\epsilon^2}\mathscr{P}^{-1}(\Delta\hat{H}_1^{*,n+1})\left(\int_\Omega T_1\phi_1^{n+1}d\boldsymbol{x} + \int_\Omega T_2\phi_2^{n+1}d\boldsymbol{x}\right) = \mathscr{P}^{-1}(r_1^n),$$

$$(3.27)\quad \phi_2^{n+1} - \frac{6}{\Sigma_2\epsilon^2}\mathscr{P}^{-1}(\Delta\hat{H}_2^{*,n+1})\left(\int_\Omega T_1\phi_1^{n+1}d\boldsymbol{x} + \int_\Omega T_2\phi_2^{n+1}d\boldsymbol{x}\right) = \mathscr{P}^{-1}(r_2^n).$$

Next, taking the L^2 inner product of (3.26) with T_1, and of (3.27) with T_2, we obtain

$$(3.28) \qquad \begin{bmatrix} 1+a & a \\ b & 1+b \end{bmatrix}\begin{bmatrix} \int_\Omega T_1\phi_1^{n+1}d\boldsymbol{x} \\ \int_\Omega T_2\phi_2^{n+1}d\boldsymbol{x} \end{bmatrix} = \begin{bmatrix} \int_\Omega T_1\mathscr{P}^{-1}(r_1^n)d\boldsymbol{x} \\ \int_\Omega T_2\mathscr{P}^{-1}(r_2^n)d\boldsymbol{x} \end{bmatrix},$$

where

$$a = -\frac{6}{\Sigma_1\epsilon^2}\int_\Omega T_1\mathscr{P}^{-1}(\Delta\hat{H}_1^{*,n+1})d\boldsymbol{x}, \quad b = -\frac{6}{\Sigma_2\epsilon^2}\int_\Omega T_2\mathscr{P}^{-1}(\Delta\hat{H}_2^{*,n+1})d\boldsymbol{x}.$$

The determinant of the above system is

$$det = 1 + a + b = 1 - \sum_{i=1}^3 \frac{6}{\Sigma_i\epsilon^2}\int_\Omega \hat{H}_i^{*,n+1}\mathscr{P}^{-1}(\Delta\hat{H}_i^{*,n+1})d\boldsymbol{x}.$$

(a) $(\sigma_{12}, \sigma_{13}, \sigma_{23})=(1,1,1)$.   (b) $(\sigma_{12}, \sigma_{13}, \sigma_{23})=(1,3,1)$.   (c) $(\sigma_{12}, \sigma_{13}, \sigma_{23})=(1,1,3)$.

(d) Energy evolution.   (e) A close-up view.
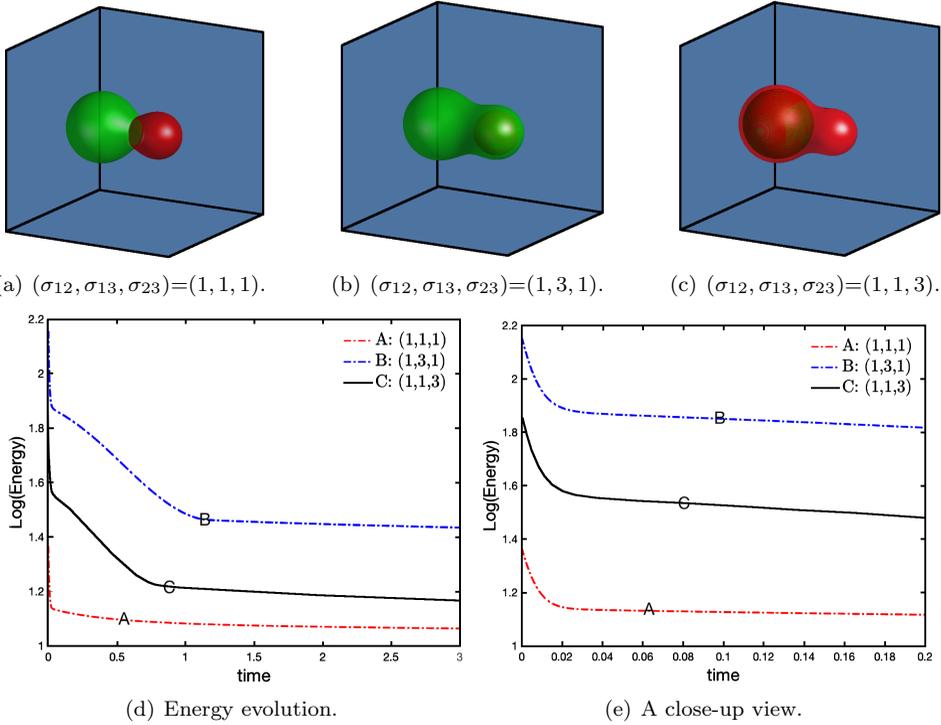
FIGURE 3.3. The equilibrium solution of the two close-by spheres driven by surface tension forces for three spreading cases where (a) $(\sigma_{12}, \sigma_{13}, \sigma_{23})=(1,1,1)$, (b) $(\sigma_{12}, \sigma_{13}, \sigma_{23})=(1,1,3)$, and (c) $(\sigma_{12}, \sigma_{13}, \sigma_{23})=(1,3,1)$, (d) Time evolution of the logarithm of the total free energy for the three cases, and (e) A close-up view of the energy evolution.

Since $-\mathscr{P}^{-1}(\Delta)$ is a positive definite operator, we have $det > 0$ which implies the linear system (3.28) is uniquely solvable. Once, we obtain $\int_\Omega T_i \phi_i^{n+1} d\boldsymbol{x}$ from (3.28), we can then solve ϕ_i^{n+1}, $(i = 1, 2)$ from (3.27).

We performed 3D simulations to investigate the effect of surface tension forces on two close-by spheres with different radius. The computational domain is set to be $(0, 2)^3$ with periodic boundary conditions. The space is discretized by using 257^3 Fourier modes. The initial conditions read as

$$\phi_i^0(\boldsymbol{x}) = \tanh(\frac{r_i - \sqrt{(x-x_i)^2+(y-y_i)^2+(z-z_i)^2}}{\epsilon}), i = 1, 2; \quad \phi_3^0(\boldsymbol{x}) = 1 - \phi_1^0(\boldsymbol{x}) - \phi_2^0(\boldsymbol{x}),$$

where $\epsilon = 0.025$, $r_1 = 0.4$, $r_2 = 0.3$, $x_1 = 1.4$, $x_2 = 0.7$, and $y_1 = y_2 = z_1 = z_2 = 1$. We set $M = 1e-2$ and $\delta t = 1e-4$. In Fig. 3.3(a-c), we plot the isosurfaces of $\{\phi_1 = 0.5\}$ and $\{\phi_2 = 0.5\}$ at the steady state with surface tension parameters of $(\sigma_{12}, \sigma_{13}, \sigma_{23}) = (1,1,1)$, $(1,3,1)$, and $(1,1,3)$, respectively. In Fig. 3.3(d) and (e), we plot the time evolutions of the logarithms of the original total free energy (3.15) for these 3D simulations. More details about these simulations can be found in [**58**].

4. Stabilized IEQ and SAV approaches for problems
with highly stiff nonlinear terms

In this section, we consider several challenging gradient flows that are not easy to deal with by using the IEQ and SAV methods directly. These models are either with very strong anisotropy so that spatial oscillations can induce severe constraints on the time step, or with very high stiffness issue due to the model parameters. While IEQ and SAV methods applied to these models are formally unconditionally energy stable, but exceedingly small time steps are needed to achieve reasonable accuracy. To fix such an inherent deficiency, we combine the IEQ and SAV approaches with the stabilization technique to construct stabilized-IEQ (S-IEQ) and stabilized-SAV (S-SAV) methods. More precisely, by adding one or several suitable linear stabilization terms and treating involved nonlinear terms in the semi-explicit way, we can construct unconditionally energy stable schemes which are easily solvable and can produce accurate results with reasonable time steps.

4.1. Anisotropic Cahn-Hilliard model. In [41, 43], the authors considered an anisotropic Cahn-Hilliard model where a sufficiently big anisotropic coefficient is introduced to allow the formation of faceted pyramids on nanoscale crystal surfaces.

Let ϕ be an order parameter which takes the values ± 1 in the two phases with a smooth transitional layer of thickness ϵ. We consider the total free energy as follows,

$$(4.1) \qquad E(\phi) = \int_\Omega \left(\gamma(\boldsymbol{n})(\frac{1}{2}|\nabla\phi|^2 + \frac{1}{\epsilon^2}F(\phi)) + \frac{\beta}{2}(\Delta\phi)^2 \right) d\boldsymbol{x},$$

where $\gamma(\boldsymbol{n})$ is a function describing the anisotropic property, and $\boldsymbol{n}$ is the interface normal defined by $\boldsymbol{n} = \frac{\nabla\phi}{|\nabla\phi|}$, $F(\phi) = \frac{1}{4}(\phi^2 - 1)^2$. The anisotropic function may takes the fourfold form that reads as

$$(4.2) \qquad \gamma(\boldsymbol{n}) = 1 + \alpha\cos(4\Theta) = 1 + \alpha(4\sum_{i=1}^{d} n_i^4 - 3),$$

where Θ denotes the orientation angle of the interfacial normal to the interface. The non-negative parameter α in (4.2) describes the intensity of anisotropy. When $\alpha = \beta = 0$, the system degenerates to the isotropic Cahn-Hilliard model.

The anisotropic Cahn-Hilliard system is then the H^{-1} gradient flow of the total free energy $E(\phi)$:

$$(4.3) \qquad \phi_t = M\Delta\mu,$$

$$(4.4) \qquad \mu = \frac{1}{\epsilon^2}\gamma(\boldsymbol{n})f(\phi) - \nabla\cdot\mathbf{m} + \beta\Delta^2\phi,$$

where $f(\phi) = F'(\phi)$, M is the mobility parameter. The vector field $\mathbf{m}$ is defined as

$$\mathbf{m} = \gamma(\boldsymbol{n})\nabla\phi + \frac{\mathbb{P}\nabla_{\boldsymbol{n}}\gamma(\boldsymbol{n})}{|\nabla\phi|}(\frac{1}{2}|\nabla\phi|^2 + \frac{1}{\epsilon^2}F(\phi)),$$

where the matrix $\mathbb{P} = \mathbb{I} - \boldsymbol{n}\boldsymbol{n}^T$.

The total free energy in (4.1) is naturally split into a linear part and a nonlinear part so we can apply IEQ or SAV approaches based on this splitting. We take the

SAV approach and define an auxiliary variable $u(t)$ as follows:

$$u(t) = \sqrt{\int_\Omega \gamma(\boldsymbol{n})\left(\frac{1}{2}|\nabla\phi|^2 + \frac{1}{\epsilon^2}F(\phi)\right)d\boldsymbol{x} + C_0},$$

where C_0 is any constant that ensures the radicand positive. Thus the total free energy (4.14) can be rewritten as

$$(4.5) \qquad E(u, \phi) = \frac{\beta}{2}\int_\Omega (\Delta\phi)^2 d\boldsymbol{x} + u^2 - C_0,$$

Using the new variable u, we then have the following equivalent H^{-1} gradient flow:

$$(4.6) \qquad \phi_t = M\Delta\mu,$$

$$(4.7) \qquad \mu = H(\phi)u + \beta\Delta^2\phi,$$

$$(4.8) \qquad u_t = \frac{1}{2}\int_\Omega H(\phi)\phi_t d\boldsymbol{x},$$

where

$$H(\phi) = \frac{\frac{1}{\epsilon^2}\gamma(\boldsymbol{n})f(\phi) - \nabla\cdot\boldsymbol{m}}{\sqrt{\int_\Omega \gamma(\boldsymbol{n})\left(\frac{1}{2}|\nabla\phi|^2 + \frac{1}{\epsilon^2}F(\phi)\right)d\boldsymbol{x} + C_0}}.$$

We present below the stabilized SAV scheme based on BDF2 for (4.6)-(4.8).

Assuming ϕ^n, u^n and ϕ^{n-1}, u^{n-1} are known, we update ϕ^{n+1}, u^{n+1} by solving

$$(4.9) \qquad \frac{3\phi^{n+1} - 4\phi^n + \phi^{n-1}}{2\delta t} = M\Delta\mu^{n+1},$$

$$(4.10) \quad \mu^{n+1} = H^{*,n+1}u^{n+1} + \beta\Delta^2\phi^{n+1}$$

$$(4.11) \qquad\qquad + \frac{S_1}{\epsilon^2}(\phi^{n+1} - 2\phi^n + \phi^{n-1}) - S_2\Delta(\phi^{n+1} - 2\phi^n + \phi^{n-1}),$$

$$(4.12) \quad 3u^{n+1} - 4u^n + u^{n-1} = \frac{1}{2}\int_\Omega H^{*,n+1}(3\phi^{n+1} - 4\phi^n + \phi^{n-1})d\boldsymbol{x},$$

where $H^{*,n+1} = H(\phi^{*,n+1})$ and S_1, S_2 are two positive stabilizing parameters. Note that with $S_1 = S_2 = 0$, the above scheme reduces to the usual SAV scheme based on BDF2. Adding stabilization terms is a commonly used technique (see, for instance, [37] for the isotropic model and [8] for the anisotropic model). The two stabilization terms associated with S_1 and S_2 are of second-order so that the above scheme is still of second-order.

Similar to the SAV scheme, we can also prove the following stability result for the above stabilized SAV scheme [7]:

THEOREM 4.1. *Let $S_1, S_2 \geq 0$. The scheme (4.9)-(4.12) is unconditionally energy stable in the sense that the following discrete energy dissipation law is satisfied:*

$$\frac{1}{\delta t}(E^{n+1} - E^n) \leq -M\|\nabla\mu^{n+1}\|^2 \leq 0,$$

where

$$E^{n+1} = \frac{(u^{n+1})^2 + (2u^{n+1} - u^n)^2}{2} + \frac{\beta}{2}\left(\frac{\|\Delta\phi^{n+1}\|^2 + \|2\Delta\phi^{n+1} - \Delta\phi^n\|^2}{2}\right)$$
$$+ \frac{S_1}{\epsilon^2}\frac{\|\phi^{n+1} - \phi^n\|^2}{2} + S_2\frac{\|\nabla\phi^{n+1} - \nabla\phi^n\|^2}{2}.$$

(a) $\delta t = 1\text{e}{-}5$.

(b) $\delta t = 1\text{e}{-}6$.

(c) $\delta t = 1\text{e}{-}7$.

(d) $\delta t = 1\text{e}{-}8$.
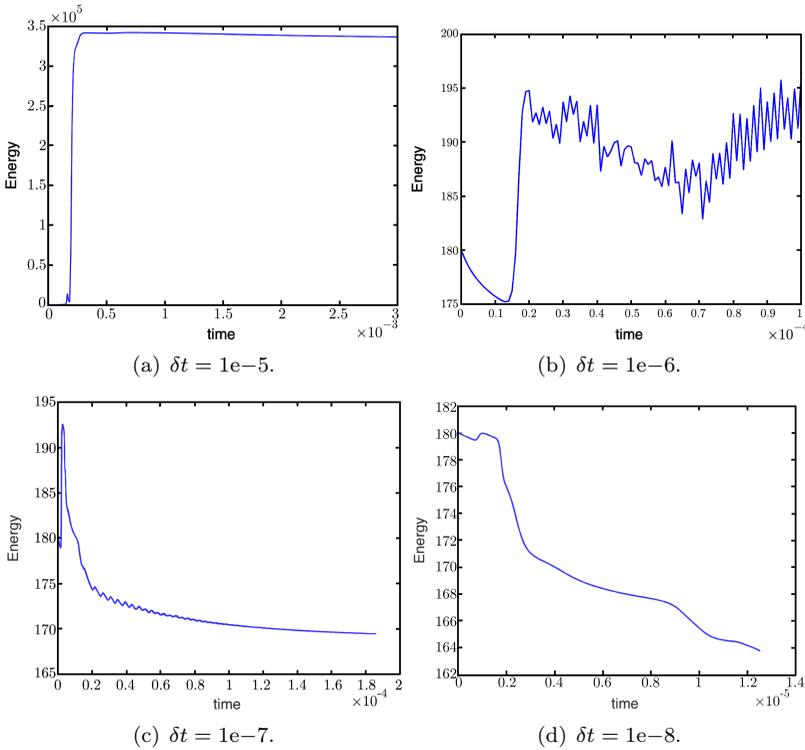
FIGURE 4.1. Time evolution of the total free energy functional (4.14) for the anisotropic linear regularization model by using the non-stabilized scheme SAV ($S_1 = S_2 = S_3 = 0$) for four time steps of 1e−5, 1e−6, 1e−7, and 1e−8.

We take $\Omega = [0, 2\pi)^2$ with periodic boundary conditions, and take the following initial condition

$$(4.13) \qquad \phi^0 = -\tanh\Big(\frac{\sqrt{(x-\pi)^2+(y-\pi)^2}-1.7}{2\epsilon}\Big),$$

with $\epsilon = 6\text{e}{-}2$. We first examine whether the non-stabilized SAV scheme ($S_1 = S_2 = 0$) is effective for solving the anisotropic model. In Fig. 4.1, we present the time evolutions of the free energy (4.1) by using four time steps $\delta t = 1\text{e}{-}5$, 1e−6, 1e−7, and 1e−8. We observe that the free energy either increases or oscillates even when very tiny time steps are used, which implies that the non-stabilized SAV scheme is not effective in dealing with the anisotropic model.

Then we solve the anisotropic model by using the stabilized SAV (SSAV) scheme. By using the time step $\delta t = 1\text{e}{-}4$, we test performance of three combinations of stabilizers: (I) $S_1 = 4, S_2 = 0$, (II) $S_1 = 4, S_2 = 4$, and (III) $S_1 = 0, S_2 = 4$. In Fig. 4.2(a), the evolutions of the free energy functional (4.1) are shown for these three cases. For (I) and (III), the energies either present some non-physical oscillations or increase with time. These unreasonable phenomena can be eliminated efficiently for combination (II), that means the values in (II) can suppress high-frequency oscillations efficiently. In Fig. 4.2(b), we show the evolution of the two

(a) Energy evolutions with three combinations of stabilizers using the stabilized scheme SSAV.

(b) Energy evolutions with time.

(c) Snapshots of ϕ.
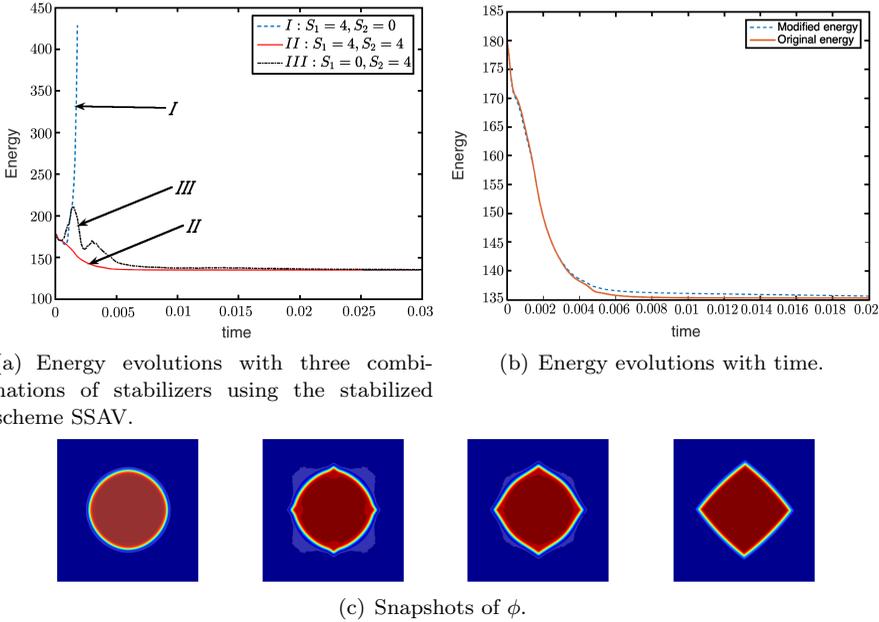
FIGURE 4.2. (a) Energy evolutions with three combinations of stabilizers; (b) Time evolution of the two free energy functionals, the original energy (4.1) and the modified energy (4.5); (c) the 2D dynamical evolution of the phase variable ϕ by using the initial condition (4.13) and the SSAV scheme.

free energy functionals (4.1) and (4.5) until the equilibrium. With a very slight difference, these two energy functionals decay to the equilibrium at around $t = 0.01$. In Fig. 4.2(c), with the stabilizer (II) and time step $\delta t = 1\mathrm{e}{-4}$, we show the dynamics of how a 2D circular shape interface with full orientations evolves to an anisotropic pyramid with missing orientations at four corners. Snapshots of the phase-field variable ϕ are taken at $t = 5\mathrm{e}{-4}$, $1.5\mathrm{e}{-3}$, $2.5\mathrm{e}{-3}$, and $2\mathrm{e}{-2}$. More detailed simulations can be found in [**7**, **48**].

4.2. Anisotropic dendritic model. The phase-field method, as a powerful tool for simulating free interfacial motions, had been widely used for investigating the process of dendritic crystal growth, see the pioneering modeling work of Halperin, Kobayashi, and Collins et. al. in[**13**, **23**, **24**].

Let $\phi(\boldsymbol{x}, t)$ be an order parameter to label the liquid and solid phase, where $\phi = 1$ for the solid and $\phi = -1$ for the fluid. Then, the total free energy describing the anisotropic dendritic crystal growth is

$$(4.14) \qquad E(\phi, T) = \int_\Omega \Big(\frac{1}{2} |\kappa(\nabla\phi)\nabla\phi|^2 + \frac{F(\phi)}{4\epsilon^2} + \frac{\lambda}{2\epsilon K} T^2 \Big) d\boldsymbol{x},$$

in which, ϵ, λ and K are all positive parameters, $T(\boldsymbol{x}, t)$ is the temperature, $F(\phi) = (\phi^2 - 1)^2$ is the double well potential, $\kappa(\nabla\phi)$ is a function describing the anisotropic property that depends on the direction of the outer normal vector $\boldsymbol{n}$ which is the interface normal defined as $\boldsymbol{n} = -\frac{\nabla\phi}{|\nabla\phi|}$. For the 2D system, the anisotropy

coefficient $\kappa(\nabla\phi)$ is usually given by

$$\kappa(\nabla\phi) = 1 + \epsilon_4 \cos(m\Theta),$$

where m is the number of folds of anisotropy, ϵ_4 is the parameter for the anisotropy strength, and $\Theta = \arctan(\frac{\phi_y}{\phi_x})$. When $m = 4$ (i.e., fourfold anisotropy), for instance, $\kappa(\nabla\phi)$ can be easily reformulated in terms of the phase-field variable ϕ, namely, for 2D,

$$\kappa(\nabla\phi) = (1 - 3\epsilon_4)\Big(1 + \frac{4\epsilon_4}{1 - 3\epsilon_4}\frac{\phi_x^4 + \phi_y^4}{|\nabla\phi|^4}\Big).$$

The dynamics of the anisotropic dendritic crystal growth is governed by the following system:

$$(4.15)\quad \tau(\phi)\phi_t = -\frac{\delta E}{\delta\phi} - \frac{\lambda}{\epsilon}p'(\phi)T,$$

$$= \nabla \cdot (\kappa^2(\nabla\phi)\nabla\phi + \kappa(\nabla\phi)|\nabla\phi|^2\mathbf{\Psi}(\phi)) - \frac{f(\phi)}{\epsilon^2} - \frac{\lambda}{\epsilon}p'(\phi)T,$$

$$(4.16)\quad T_t = D\Delta T + Kp'(\phi)\phi_t,$$

where $\tau(\phi) > 0$ is the mobility function, D is the diffusion rate of the temperature, the function $p(\phi)$ accounts for the generation of latent heat and it is a phenomenological functional taking the form preserving the minima of ϕ at ± 1 independently of the local value of u. For $p(\phi)$, there are two common choices: $p(\phi) = \frac{1}{5}\phi^5 - \frac{2}{3}\phi^3 + \phi$ and $p'(\phi) = (1 - \phi^2)^2$ (cf. [**24**, **27**]); or $p(\phi) = \phi - \frac{1}{3}\phi^3$ and $p'(\phi) = 1 - \phi^2$ (cf. [**42**]), $\mathbf{\Psi}(\phi)$ is the variational derivative of $\kappa(\nabla\phi)$.

Note that the above system is not really a gradient flow of the free energy (4.14) due to the two phenomenological terms associated with $p'(\phi)$. But it still satisfies a dissipative energy law. Indeed, by taking the L^2 inner product of (4.15) with ϕ_t, and of (4.16) with $\frac{\lambda}{\epsilon K}T$, using the integration by parts and combining the obtained two equalities, we obtain

$$\frac{d}{dt}E(\phi, T) = -\|\sqrt{\tau(\phi)}\phi_t\|^2 - \frac{\lambda D}{\epsilon K}\|\nabla T\|^2 \leq 0.$$

As in the case of anisotropic Cahn-Hilliard system, we can apply the stabilized IEQ or SAV approach. Due to the terms $\tau(\phi)\phi_t$ and $p'(\phi)T$ in the system (4.15)-(4.16) which can not be treated explicitly, the SAV approach will also lead to linear system with variable coefficients, so we use the IEQ approach which offers stronger coupling, and define

$$U = \sqrt{\frac{1}{2}|\kappa(\nabla\phi)\nabla\phi|^2 + \frac{1}{4\epsilon^2}F(\phi) + C_0},$$

where C_0 is any constant that can ensure the radicand positive. Thus the total free energy (4.14) can be rewritten as

$$E(\phi, U, u) = \int_\Omega (U^2 + \frac{\lambda}{2\epsilon K}T^2 - C_0)d\boldsymbol{x},$$

(a) Energy evolutions with various time steps.

(b) A close-up view.
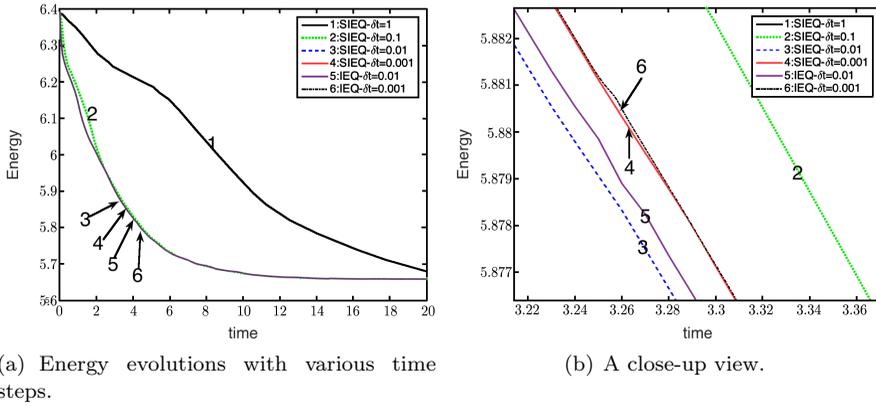
FIGURE 4.3. Time evolutions of the total free energy functional using the two schemes, IEQ and SIEQ, for four different time steps $\delta t = 1$, 1e−1, 1e−2, and 1e−3 (the IEQ scheme with $\delta t = 1$ and 1e−1 leads to totally wrong results so they are not included). The left subfigure (a) is the energy profile for $t \in [0, 20]$, and the right subfigure (b) is a close-up view for $t \in [3.21, 3.37]$.

and we can formulate an equivalent system to (4.15)-(4.16) as follows:

$$(4.17) \qquad \tau(\phi)\phi_t = -Z(\phi)U - \frac{\lambda}{\epsilon}p'(\phi)T,$$

$$(4.18) \qquad U_t = \frac{1}{2}Z(\phi)\phi_t,$$

$$(4.19) \qquad T_t = D\Delta T + Kp'(\phi)\phi_t,$$

where

$$Z(\phi) = \frac{-\nabla \cdot (\kappa^2(\nabla\phi)\nabla\phi + \kappa(\nabla\phi)|\nabla\phi|^2\boldsymbol{\Psi}(\phi)) + \frac{1}{\epsilon^2}f(\phi)}{\sqrt{\frac{1}{2}|\kappa(\nabla\phi)\nabla\phi|^2 + \frac{1}{4\epsilon^2}F(\phi) + C_0}}.$$

Then, a second-order stabilized IEQ scheme for the above system (4.17)-(4.19) is:

Assuming ϕ^n, T^n, U^n and $\phi^{n-1}, T^{n-1}, U^{n-1}$ are known, we update $\phi^{n+1}, T^{n+1}, U^{n+1}$ by solving the following linear coupled system:

$$(4.20) \quad \tau(\phi^{*,n+1})\frac{3\phi^{n+1} - 4\phi^n + \phi^{n-1}}{2\delta t} = -Z^{*,n+1}U^{n+1} - \frac{\lambda}{\epsilon}p'(\phi^{*,n+1})T^{n+1}$$

$$+ \frac{S_1}{\epsilon^2}(\phi^{n+1} - 2\phi^n + \phi^{n-1}) - S_2\Delta(\phi^{n+1} - 2\phi^n + \phi^{n-1}),$$

$$(4.21) \quad 3U^{n+1} - 4U^n + U^{n-1} = \frac{1}{2}Z^{*,n+1}(3\phi^{n+1} - 4\phi^n + \phi^{n-1}),$$

$$(4.22) \quad \frac{3T^{n+1} - 4T^n + T^{n-1}}{2\delta t} - D\Delta T^{n+1} = Kp'(\phi^{*,n+1})\frac{3\phi^{n+1} - 4\phi^n + \phi^{n-1}}{2\delta t},$$

where $Z^{*,n+1} = Z(\phi^{*,n+1})$, and S_i $(i = 1, 2)$ are positive stabilizing parameters.

Note that if we replace the variable coefficients $\tau(\phi^{*,n+1})$, $p'(\phi^{*,n+1})$ and $Z^{*,n+1}$ in the above by constants, e.g., their average values, we can solve the corresponding system easily with a Fourier-spectral method. Then, the above system can be
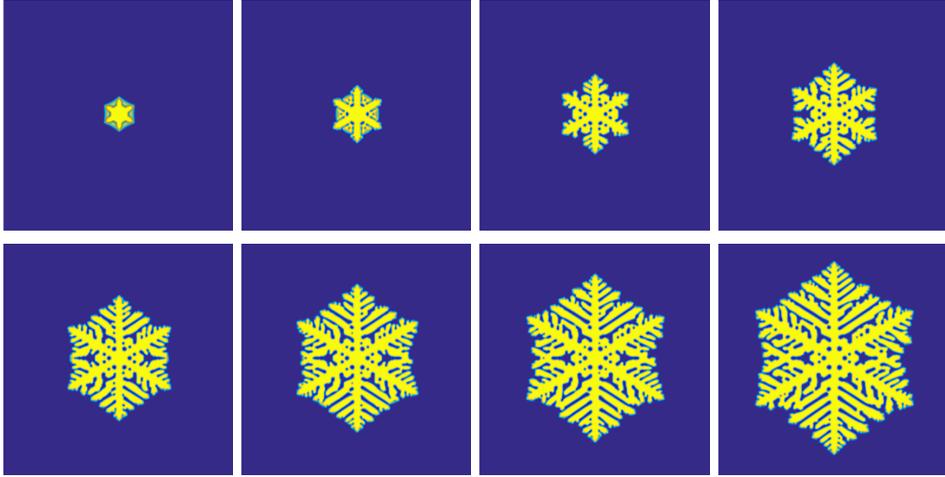
FIGURE 4.4. The 2D dynamical evolutions of dendritic crystal growth process with the sixfold anisotropy.

efficiently solved by using a preconditioned conjugate gradient type iteration using the corresponding system with constant coefficients as a preconditioner.

Similarly, one can prove the following stability results [**50**]:

THEOREM 4.2. *Let $S_1, S_2 > 0$. The scheme (4.20)-(4.22) is unconditionally energy stable in the sense that the following discrete energy dissipation law is satisfied:*

$$\frac{1}{\delta t}(E^{n+1} - E^n) \leq -\|\sqrt{\tau(\phi^{*,n+1})}\frac{3\phi^{n+1} - 4\phi^n + \phi^{n-1}}{2\delta t}\|^2 - \frac{\lambda D}{\epsilon K}\|\nabla u^{n+1}\|^2 \leq 0,$$

where

$$E^{n+1} = \frac{\|U^{n+1}\|^2 + \|2U^{n+1} - U^n\|^2}{2} + \frac{\lambda}{2\epsilon K}\Big(\frac{\|u^{n+1}\|^2 + \|2u^{n+1} - u^n\|^2}{2}\Big)$$
$$+ \frac{S_1}{\epsilon^2}\frac{\|\phi^{n+1} - \phi^n\|^2}{2} + S_2\frac{\|\nabla\phi^{n+1} - \nabla\phi^n\|^2}{2}.$$

In Fig. 4.3, we compare the evolution of the free energy functionals using the IEQ and stabilized IEQ (SIEQ) schemes with four different time steps $\delta t = 1, 1e-1, 1e-2,$ and $1e-3$. For larger times steps $\delta t = 1, 1e-1$, the IEQ scheme leads to totally wrong results. But when we add two stabilizers in, all four energy curves generated by the SIEQ scheme decay monotonically. In Fig. 4.4, we perform a simulation with the sixfold anisotropic entropy coefficient. We observe that numerous sub-branches form on each main branch, and lead eventually to a snowflake pattern. More detailed numerical simulations can be found in [**6, 50, 60**].

4.3. Modified PFC model with a strong nonlinear vacancy potential (VMPFC). The VMPFC model [**5, 39, 40**] is different from the classical PFC model (3.4)-(3.6) in the following two aspects, (i) the second-order time derivative is introduced into the PDE in order to include both diffusive dynamics and elastic interactions, and (ii) a strong nonlinear penalization potential is added in the free energy in order to induce vacancies between atoms by penalizing the negative value of the phase-field variable.

The total free energy of the VMPFC system is

$$(4.23) \qquad E(\phi) = \int_\Omega \Big(\frac{\phi}{2} \mathcal{L}_1^2 (\mathcal{L}_2^2 + r^2)\phi + F(\phi) + F_{vac}(\phi) \Big) d\boldsymbol{x},$$

where $F(\phi) = \frac{1}{4}\phi^4 - \frac{\eta}{2}\phi^2$ is the double-well potential, and

$$F_{vac}(\phi) = \frac{h_{vac}}{3}(|\phi|^3 - \phi^3),$$

is the vacancy potential that penalizes negative values of ϕ with $h_{vac} \gg 1$ being the penalization parameter. It is easy to see that that $F(\phi) + F_{vac}(\phi)$ is bounded from below for any ϕ.

We consider the following H^{-1} pseudo-gradient flow of the above free energy:

$$(4.24) \qquad \alpha\phi_{tt} + \beta\phi_t = M\Delta\mu,$$

$$(4.25) \qquad \mu = \mathcal{L}_1^2(\mathcal{L}_2^2 + r^2)\phi + f(\phi) + f_{vac}(\phi),$$

where $M > 0$ is the mobility constant, α and β are two non-negative parameters, $f(\phi) = F'(\phi) = \phi^3 - \epsilon\phi$ and $f_{vac}(\phi) = F'_{vac}(\phi) = h_{vac}(|\phi| - \phi)\phi$. When $\alpha = h_{vac} = 0$, the model (4.24)-(4.25) reduces to the classical PFC model (3.2)-(3.3).

In order to fit the above model in our general setting, we introduce a new variable $\psi = \phi_t$, and adopt the SAV approach. More precisely, we define an auxiliary non-local function

$$u(t) = \sqrt{\int_\Omega (F(\phi) + F_{vac}(\phi))d\boldsymbol{x} + C_0},$$

where C_0 is a constant such the radicand is strictly positive, and rewrite (4.24)-(4.25) as

$$(4.26) \qquad \alpha\psi_t + \beta\psi = M\Delta\mu,$$

$$(4.27) \qquad \mu = (\Delta + 1)^2\phi + Ku,$$

$$(4.28) \qquad \psi = \phi_t,$$

$$(4.29) \qquad u_t = \frac{1}{2}\int_\Omega K\phi_t d\boldsymbol{x},$$

where

$$K = \frac{f(\phi) + f_{vac}(\phi)}{\sqrt{\int_\Omega (F(\phi) + F_{vac}(\phi))d\boldsymbol{x} + C_0}}.$$

Then, we can construct a second-order stabilized SAV scheme for (4.26)-(4.29) as follows.

Having computed $(\phi, \psi, u)^{n-1}$ and $(\phi, \psi, u)^n$, we compute $(\phi, \psi, u)^{n+1}$ as follows.

$$(4.30) \qquad \alpha\frac{3\psi^{n+1} - 4\psi^n + \psi^{n-1}}{2\delta t} + \beta\psi^{n+1} = M\Delta\mu^{n+1},$$

$$(4.31) \qquad \mu^{n+1} = \mathcal{L}_1^2(\mathcal{L}_2 + r^2)^2\phi^{n+1} + K^{\star,n+1}u^{n+1} + S(\phi^{n+1} - \phi^{\star,n+1}),$$

$$(4.32) \qquad \psi^{n+1} = \frac{3\phi^{n+1} - 4\phi^n + \phi^{n-1}}{2\delta t},$$

$$(4.33) \qquad 3u^{n+1} - 2u^n + u^{n-1} = \frac{1}{2}\int_\Omega K^{\star,n+1}(3\phi^{n+1} - 4\phi^n + \phi^{n-1})d\boldsymbol{x},$$
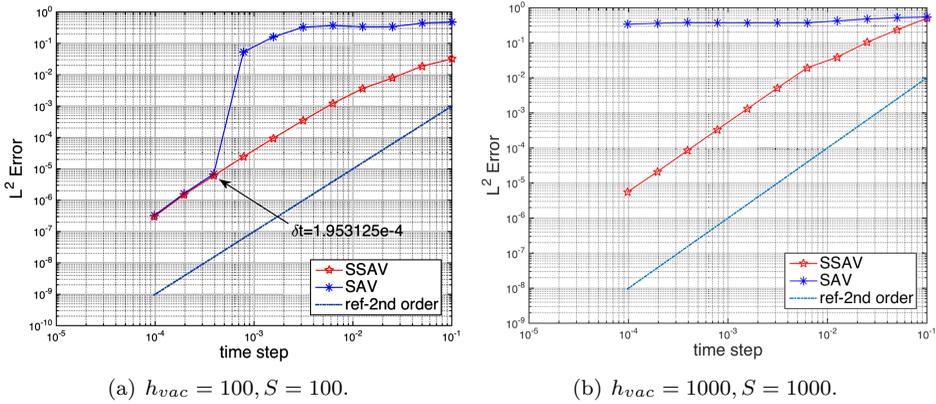
FIGURE 4.5. The L^2 numerical errors for the phase-field variable ϕ that are computed using the schemes SSAV and SAV for the mesh refinement test in time with the initial conditions (4.34). The penalization parameters h_{vac} and the stabilization parameter S are set as (a) $h_{vac} = S = 100$ and (b) $h_{vac} = S = 1000$.

where S is a positive stabilization parameter, and $K^{\star,n+1} = K(\phi^{\star,n+1})$ with $\phi^{\star,n+1} = 2\phi^n - \phi^{n-1}$.

The above system can be efficiently solved using the same procedure for (2.18)-(2.20) presented in Section 2, which leads to a linear system with constant coefficients that can be solved easily. We refer to [**62**] for more detail.

As for the stability, we can prove the following result [**62**]:

THEOREM 4.3. *Let $S \geq 0$. The scheme* (4.30)-(4.33) *is unconditionally energy stable in the sense that the following discrete energy dissipation law is satisfied:*

$$E^{n+1} \leq E^n - \delta t \frac{\beta}{M} \|\nabla p^{n+1}\|^2,$$

where, for any integer $k \geq 0$, the discrete energy E^k is defined as

$$E^k = \frac{1}{2} \left(\frac{\|\mathcal{L}_1 \mathcal{L}_2 \phi^k\|^2 + \|2\mathcal{L}_1 \mathcal{L}_2 \phi^k - \mathcal{L}_1 \mathcal{L}_2 \phi^{k-1})\|^2}{2} \right)$$

$$+ \frac{r^2}{2} \left(\frac{\|\mathcal{L}_1 \phi^k\|^2 + \|2\mathcal{L}_1 \phi^k - \mathcal{L}_1 \phi^{k-1})\|^2}{2} \right) + S \frac{\|\phi^k - \phi^{k-1}\|^2}{2}$$

$$+ \frac{\alpha}{2M} \left(\frac{\|\nabla p^k\|^2 + \|2\nabla p^k - \nabla p^{k-1}\|^2}{2} \right) + \frac{(u^k)^2 + (2u^k - u^{k-1})^2}{2},$$

and p^k is defined as $p^k = \Delta^{-1} \psi^k$.

We now present some numerical results obtained using the above scheme with $S = 0$ (SAV) and with $S > 0$ (SSAV). We take $\Omega = (0, 128)^2$ and assume the periodic boundary conditions. We take the initial condition to be

(4.34) $$\phi^0(x,y) = \sin(\frac{8\pi}{128}x)\cos(\frac{8\pi}{128}y), \psi^0(x,y) = 0,$$

and choose the solution computed by the SSAV scheme with the time step size $\delta t = 1e-9$ as the benchmark solution. The L^2 errors of the phase variable between

(a) SSAV.   (b) SAV.
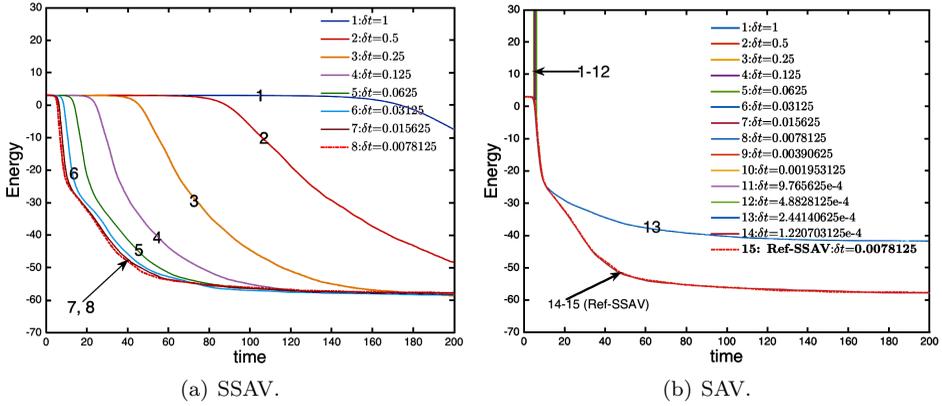
FIGURE 4.6. Time evolution of the total free energy (4.23) computed by the two schemes SSAV and SAV with various time steps. The penalization parameter is $h_{vac} = 5e5$ and the stabilization parameter is $S = 500$. (Note: in the subfigure (b), we use the energy curve computed by the scheme SSAV with $\delta t = 0.0078125$ as the reference solution.)
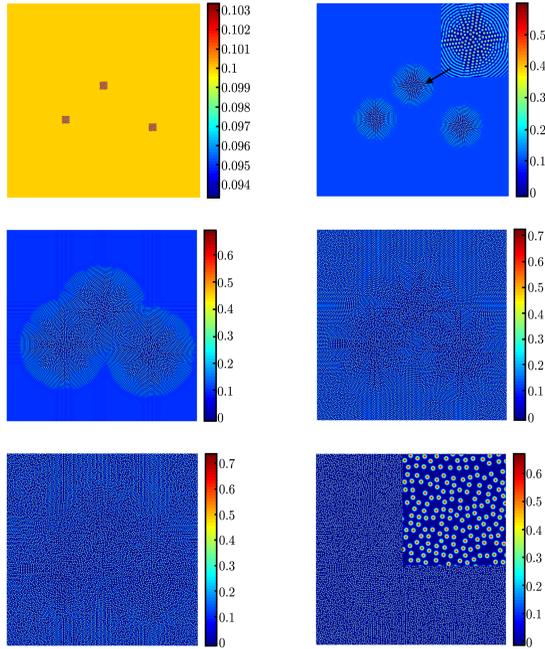
FIGURE 4.7. The dynamical behaviors of the crystal growth with three initial crystallites arbitrarily deposited in a supercooled liquid for the case of vacancies. The parameters are $h_{vac} = 3000, \epsilon = 0.9, M = 1, \alpha = 1, \beta = 1, S = 2$. Snapshots of the numerical approximation of ϕ are taken at $t = 0, 25, 50, 75, 100,$ and 1000.

the numerical solution and the exact solution at $t = 2$ with different time step sizes are shown in Fig. 4.5 where $h_{vac} = S = 100$ and $h_{vac} = S = 1000$ are used, respectively. We observe that (i) even though the SAV (non-stabilized) scheme is stable for all tested time steps, it is not accurate for larger time steps, and (ii) the stabilized scheme SSAV is stable for all tested time steps and leads to second-order accuracy with good approximations for all time steps.

Next, we take the initial condition to be

$$\phi^0(x, y) = 0.06 + 0.001 \operatorname{rand}(x, y), \psi^0(x, y) = 0,$$

where $\operatorname{rand}(x, y)$ is the random number in the range of $[-1, 1]$. We set the penalization parameter to $h_{vac} = 5\text{e}5$ and the stabilization parameter $S = 500$. the evolution curves of the total free energy for these two schemes are plotted in Fig. 4.6. We find that the scheme SSAV is stable and the free energy decays for all tested time steps, but the free energy computed by using the non-stabilized scheme SAV decays only when $\delta t \lesssim 2.4\text{e}{-}4$.

As the last example, we set $h_{vac} = 3000$ with the three randomly deposited crystallites as initial conditions, and plot the results in Fig. 4.7. We observe that the atoms are formed but periodic patterns vanish and vacancies appear almost everywhere, which can be seen clearly in the inset figures.

5. Concluding remarks

We presented in this note the IEQ and SAV approaches in a unified framework, and show that for a large class of gradient flows or conservative systems, they lead to linear, unconditionally energy stable and al least second-order schemes. For the SAV schemes, these linear systems can be further decoupled into a set of linear systems with constant coefficients so that they are extremely efficient.

We showed that the IEQ and SAV approaches can be directly applied to problems with moderately stiff nonlinear terms, but for problems with highly stiff nonlinear terms, suitable stabilizations are needed to avoid exceedingly small time steps. While we only discussed the applications of IEQ and SAV approaches to gradient flows, they framework presented in this note also applies to Hamiltonian systems (cf. [**4**, **25**]) for which the second-order IEQ and SAV schemes based on Crank-Nicolson lead to linear and unconditionally energy-conserving schemes.

The IEQ and SAV approaches have also been extended to deal with other problems which are not driven by free energy or a Hamiltonian. For examples, a strategy for numerical approximations of general thermodynamical systems using the energy quadratization (EQ) approach is presented in [**64**], and the SAV approach is extended to construct efficient numerical schemes for incompressible Navier-Stokes equations in [**31**] and for two-phase flows with different densities in [**59**].

References

[1] A. Baskaran, J. S. Lowengrub, C. Wang, and S. M. Wise, *Convergence analysis of a second order convex splitting scheme for the modified phase field crystal equation*, SIAM J. Numer. Anal. **51** (2013), no. 5, 2851–2873, DOI 10.1137/120880677. MR3118257

[2] F. Boyer and C. Lapuerta, *Study of a three component Cahn-Hilliard flow model*, M2AN Math. Model. Numer. Anal. **40** (2006), no. 4, 653–687, DOI 10.1051/m2an:2006028. MR2274773

[3] F. Boyer and S. Minjeaud, *Numerical schemes for a three component Cahn-Hilliard model*, ESAIM Math. Model. Numer. Anal. **45** (2011), no. 4, 697–738, DOI 10.1051/m2an/2010072. MR2804656

[4] J. Cai and J. Shen, *Two classes of linearly implicit local energy-preserving approach for general multi-symplectic Hamiltonian PDEs*, J. Comput. Phys. **401** (2020), 108975, DOI 10.1016/j.jcp.2019.108975. MR4019799

[5] P. Y. Chan, N. Goldenfeld, and J. Dantzig. Molecular dynamics on diffusive time scales from the phase-field-crystal equation. *Phys. Rev. E.*, 79:035701R, 2009.

[6] C. Chen and X. Yang, *Efficient numerical scheme for a dendritic solidification phase field model with melt convection*, J. Comput. Phys. **388** (2019), 41–62, DOI 10.1016/j.jcp.2019.03.017. MR3933270

[7] C. Chen and X. Yang, *Fast, provably unconditionally energy stable, and second-order accurate algorithms for the anisotropic Cahn-Hilliard Model*, Comput. Methods Appl. Mech. Engrg. **351** (2019), 35–59, DOI 10.1016/j.cma.2019.03.030. MR3936701

[8] F. Chen and J. Shen, *Efficient energy stable schemes with spectral discretization in space for anisotropic Cahn-Hilliard systems*, Commun. Comput. Phys. **13** (2013), no. 5, 1189–1208, DOI 10.4208/cicp.101111.110512a. MR2988885

[9] H. Chen, J. Mao, and J. Shen, *Optimal error estimates for the scalar auxiliary variable finite-element schemes for gradient flows*, Numer. Math. **145** (2020), no. 1, 167–196, DOI 10.1007/s00211-020-01112-4. MR4091597

[10] Q. Cheng and J. Shen, *Multiple scalar auxiliary variable (MSAV) approach and its application to the phase-field vesicle membrane model*, SIAM J. Sci. Comput. **40** (2018), no. 6, A3982–A4006, DOI 10.1137/18M1166961. MR3881243

[11] Q. Cheng, J. Shen, and X. Yang, *Highly efficient and accurate numerical schemes for the epitaxial thin film growth models by using the SAV approach*, J. Sci. Comput. **78** (2019), no. 3, 1467–1487, DOI 10.1007/s10915-018-0832-5. MR3934674

[12] Q. Cheng, X. Yang, and J. Shen, *Efficient and accurate numerical schemes for a hydro-dynamically coupled phase field diblock copolymer model*, J. Comput. Phys. **341** (2017), 44–60, DOI 10.1016/j.jcp.2017.04.010. MR3645544

[13] J. B. Collins and H. Levine. Diffuse interface model of diffusion-limited crystal growth. *Phys. Rev. B*, 31:6119, 1985.

[14] Q. Du and X. Feng. The phase field method for geometric moving interfaces and their numerical approximations. *arXiv preprint arXiv:1902.04924*, 2019.

[15] Q. Du and R. A. Nicolaides, *Numerical analysis of a continuum model of phase transition*, SIAM J. Numer. Anal. **28** (1991), no. 5, 1310–1322, DOI 10.1137/0728069. MR1119272

[16] K. R. Elder and Martin Grant. Modeling elastic and plastic deformations in nonequilibrium processing using phase field crystals. *Phys. Rev. E.*, 70:051605, 2004.

[17] K. R. Elder, M. Katakowski, M. Haataja, and Grant M. Modeling elasticity in crystal growth. *Phys. Rev. Lett.*, 88(24):245701, 2002.

[18] C. M. Elliott and A. M. Stuart, *The global dynamics of discrete semilinear parabolic equations*, SIAM J. Numer. Anal. **30** (1993), no. 6, 1622–1663, DOI 10.1137/0730084. MR1249036

[19] D. J. Eyre, *Unconditionally gradient stable time marching the Cahn-Hilliard equation*, Computational and mathematical models of microstructural evolution (San Francisco, CA, 1998), Mater. Res. Soc. Sympos. Proc., vol. 529, MRS, Warrendale, PA, 1998, pp. 39–46, DOI 10.1557/PROC-529-39. MR1676409

[20] X. Feng and A. Prohl, *Numerical analysis of the Allen-Cahn equation and approximation for mean curvature flows*, Numer. Math. **94** (2003), no. 1, 33–65, DOI 10.1007/s00211-002-0413-1. MR1971212

[21] H. Gómez, V. M. Calo, Y. Bazilevs, and T. J. R. Hughes, *Isogeometric analysis of the Cahn-Hilliard phase-field model*, Comput. Methods Appl. Mech. Engrg. **197** (2008), no. 49-50, 4333–4352, DOI 10.1016/j.cma.2008.05.003. MR2463665

[22] H. Gomez, der Zee Van, and G. Kristoffer. Computational phase-field modeling. In: Encyclopedia of Computational Mechanics, Second Edition. John Wiley & Sons, Ltd, ISBN 978-1-119-00379-3. 2017.

[23] B. I. Halperin, P. C. Hohenberg, and S.-K. Ma. Renormalization-group methods for critical dynamics: I. recursion relations and effects of energy conservation. *Phys. Rev. B*, 139:10, 1974.

[24] R. Hobayashi. Modeling and numerical simulations of dendritic crystal growth. *Physica D*, 63:410, 1993.

[25] C. Jiang, W. Cai, and Y. Wang, *A linearly implicit and local energy-preserving scheme for the sine-Gordon equation based on the invariant energy quadratization approach*, J. Sci. Comput. **80** (2019), no. 3, 1629–1655, DOI 10.1007/s10915-019-01001-5. MR3995980

[26] L. Ju, J. Zhang, L. Zhu, and Q. Du, *Fast explicit integration factor methods for semilinear parabolic equations*, J. Sci. Comput. **62** (2015), no. 2, 431–455, DOI 10.1007/s10915-014-9862-9. MR3299200

[27] A. Karma and W. Rappel. Phase-field model of dendritic sidebranching with thermal noise. *Phys. Rev. E*, 60:3614–3625, 1999.

[28] J. Kou, S. Sun, and X. Wang, *Linearly decoupled energy-stable numerical methods for multi-component two-phase compressible flow*, SIAM J. Numer. Anal. **56** (2018), no. 6, 3219–3248, DOI 10.1137/17M1162287. MR3876867

[29] D. Li, Z. Qiao, and T. Tang, *Characterizing the stabilization size for semi-implicit Fourier-spectral method to phase field equations*, SIAM J. Numer. Anal. **54** (2016), no. 3, 1653–1681, DOI 10.1137/140993193. MR3507555

[30] X. Li, J. Shen, and H. Rui, *Energy stability and convergence of SAV block-centered finite difference method for gradient flows*, Math. Comp. **88** (2019), no. 319, 2047–2068, DOI 10.1090/mcom/3428. MR3957886

[31] L. Lin, Z. Yang, and S. Dong, *Numerical approximation of incompressible Navier-Stokes equations based on an auxiliary energy variable*, J. Comput. Phys. **388** (2019), 1–22, DOI 10.1016/j.jcp.2019.03.012. MR3933268

[32] I. Romero, *Thermodynamically consistent time-stepping algorithms for non-linear thermo-mechanical systems*, Internat. J. Numer. Methods Engrg. **79** (2009), no. 6, 706–732, DOI 10.1002/nme.2588. MR2548522

[33] J. Shen, C. Wang, X. Wang, and S. M. Wise, *Second-order convex splitting schemes for gradient flows with Ehrlich-Schwoebel type energy: application to thin film epitaxy*, SIAM J. Numer. Anal. **50** (2012), no. 1, 105–125, DOI 10.1137/110822839. MR2888306

[34] J. Shen and J. Xu, *Convergence and error analysis for the scalar auxiliary variable (SAV) schemes to gradient flows*, SIAM J. Numer. Anal. **56** (2018), no. 5, 2895–2912, DOI 10.1137/17M1159968. MR3857892

[35] J. Shen, J. Xu, and J. Yang, *The scalar auxiliary variable (SAV) approach for gradient flows*, J. Comput. Phys. **353** (2018), 407–416, DOI 10.1016/j.jcp.2017.10.021. MR3723659

[36] J. Shen, J. Xu, and J. Yang, *A new class of efficient and robust energy stable schemes for gradient flows*, SIAM Rev. **61** (2019), no. 3, 474–506, DOI 10.1137/17M1150153. MR3989239

[37] J. Shen and X. Yang, *Numerical approximations of Allen-Cahn and Cahn-Hilliard equations*, Discrete Contin. Dyn. Syst. **28** (2010), no. 4, 1669–1691, DOI 10.3934/dcds.2010.28.1669. MR2679727

[38] J. Shen and X. Yang, *Decoupled, energy stable schemes for phase-field models of two-phase in-compressible flows*, SIAM J. Numer. Anal. **53** (2015), no. 1, 279–296, DOI 10.1137/140971154. MR3303685

[39] P. Stefanovic, M. Haataja, and N. Provatas. Phase-field crystals with elastic interactions. *Phys. Rev. Lett.*, 96:225504, 2006.

[40] P. Stefanovic, M. Haataja, and N. Provatas. Phase field crystal study of deformation and plasticity in nanocrystalline materials. *Phys. Rev. E*, 80:046107, 2009.

[41] S. Torabi, J. Lowengrub, A. Voigt, and S. Wise, *A new phase-field model for strongly anisotropic systems*, Proc. R. Soc. Lond. Ser. A Math. Phys. Eng. Sci. **465** (2009), no. 2105, 1337–1359, DOI 10.1098/rspa.2008.0385. With supplementary material available online. MR2500806

[42] S.-L. Wang and et al., *Thermodynamically-consistent phase-field models for solidification*, Phys. D **69** (1993), no. 1-2, 189–200, DOI 10.1016/0167-2789(93)90189-8. MR1245661

[43] S. Wise, J. Kim, and J. Lowengrub, *Solving the regularized, strongly anisotropic Cahn-Hilliard equation by an adaptive nonlinear multigrid method*, J. Comput. Phys. **226** (2007), no. 1, 414–446, DOI 10.1016/j.jcp.2007.04.020. MR2356365

[44] K. Wu, A. Adland, and A. Karma. Phase-field-crystal model for fcc ordering. *Phys. Rev. E*, 81:061601, 2010.

[45] X. Wu, G. J. van Zwieten, and K. G. van der Zee, *Stabilized second-order convex splitting schemes for Cahn-Hilliard models with application to diffuse-interface tumor-growth models*, Int. J. Numer. Methods Biomed. Eng. **30** (2014), no. 2, 180–203, DOI 10.1002/cnm.2597. MR3164683

[46] C. Xu, C. Chen, X. Yang, and X. He, *Numerical approximations for the hydrodynamics cou-pled binary surfactant phase field model: second-order, linear, unconditionally energy stable schemes*, Commun. Math. Sci. **17** (2019), no. 3, 835–858, DOI 10.4310/CMS.2019.v17.n3.a10. MR4001484

[47] C. Xu and T. Tang, *Stability analysis of large time-stepping methods for epitaxial growth mod-els*, SIAM J. Numer. Anal. **44** (2006), no. 4, 1759–1779, DOI 10.1137/050628143. MR2257126

[48] Z. Xu, X. Yang, H. Zhang, and Z. Xie, *Efficient and linear schemes for anisotropic Cahn-Hilliard model using the Stabilized-Invariant Energy Quadratization (S-IEQ) approach*, Com-put. Phys. Commun. **238** (2019), 36–49, DOI 10.1016/j.cpc.2018.12.019. MR3925937

[49] X. Yang, *Linear, first and second-order, unconditionally energy stable numerical schemes for the phase field model of homopolymer blends*, J. Comput. Phys. **327** (2016), 294–316, DOI 10.1016/j.jcp.2016.09.029. MR3564340

[50] X. Yang, *Efficient linear, stabilized, second-order time marching schemes for an anisotropic phase field dendritic crystal growth model*, Comput. Methods Appl. Mech. Engrg. **347** (2019), 316–339, DOI 10.1016/j.cma.2018.12.012. MR3899056

[51] X. Yang and D. Han, *Linearly first- and second-order, unconditionally energy stable schemes for the phase field crystal model*, J. Comput. Phys. **330** (2017), 1116–1134, DOI 10.1016/j.jcp.2016.10.020. MR3581509

[52] X. Yang and L. Ju, *Efficient linear schemes with unconditional energy stability for the phase field elastic bending energy model*, Comput. Methods Appl. Mech. Engrg. **315** (2017), 691–712, DOI 10.1016/j.cma.2016.10.041. MR3595274

[53] X. Yang and L. Ju, *Linear and unconditionally energy stable schemes for the binary fluid-surfactant phase field model*, Comput. Methods Appl. Mech. Engrg. **318** (2017), 1005–1029, DOI 10.1016/j.cma.2017.02.011. MR3627211

[54] X. Yang and H. Yu, *Efficient second order unconditionally stable schemes for a phase field moving contact line model using an invariant energy quadratization approach*, SIAM J. Sci. Comput. **40** (2018), no. 3, B889–B914, DOI 10.1137/17M1125005. MR3815548

[55] X. Yang and G.-D. Zhang, *Convergence Analysis for the Invariant Energy Quadratiza-tion (IEQ) Schemes for Solving the Cahn–Hilliard and Allen–Cahn Equations with Gen-eral Nonlinear Potential*, J. Sci. Comput. **82** (2020), no. 3, DOI 10.1007/s10915-020-01151-x. MR4065209

[56] X. Yang and J. Zhao, *Efficient linear schemes for the nonlocal Cahn-Hilliard equa-tion of phase field models*, Comput. Phys. Commun. **235** (2019), 234–245, DOI 10.1016/j.cpc.2018.08.012. MR3906032

[57] X. Yang, J. Zhao, and Q. Wang, *Numerical approximations for the molecular beam epitaxial growth model based on the invariant energy quadratization method*, J. Comput. Phys. **333** (2017), 104–127, DOI 10.1016/j.jcp.2016.12.025. MR3599396

[58] X. Yang, J. Zhao, Q. Wang, and J. Shen, *Numerical approximations for a three-component Cahn-Hilliard phase-field model based on the invariant energy quadratization method*, Math. Models Methods Appl. Sci. **27** (2017), no. 11, 1993–2030, DOI 10.1142/S0218202517500373. MR3691811

[59] Z. Yang and S. Dong, *An unconditionally energy-stable scheme based on an implicit aux-iliary energy variable for incompressible two-phase flows with different densities involv-ing only precomputable coefficient matrices*, J. Comput. Phys. **393** (2019), 229–257, DOI 10.1016/j.jcp.2019.05.018. MR3954060

[60] J. Zhang, C. Chen, and X. Yang, *A novel decoupled and stable scheme for an anisotropic phase-field dendritic crystal growth model*, Appl. Math. Lett. **95** (2019), 122–129, DOI 10.1016/j.aml.2019.03.029. MR3937888

[61] J. Zhang and X. Yang, *On efficient numerical schemes for a two-mode phase field crystal model with face-centered-cubic (FCC) ordering structure*, Appl. Numer. Math. **146** (2019), 13–37, DOI 10.1016/j.apnum.2019.06.017. MR3996286

[62] J. Zhang and X. Yang, *Efficient second order unconditionally stable time marching numerical scheme for a modified phase-field crystal model with a strong nonlinear vacancy potential*, Comput. Phys. Commun. **245** (2019), 106860, DOI 10.1016/j.cpc.2019.106860. MR4018557

[63] J. Zhao, Q. Wang, and X. Yang, *Numerical approximations for a phase field dendritic crystal growth model based on the invariant energy quadratization approach*, Internat. J. Numer. Methods Engrg. **110** (2017), no. 3, 279–300, DOI 10.1002/nme.5372. MR3633666

[64] J. Zhao, X. Yang, Y. Gong, X. Zhao, X. Yang, J. Li, and Q. Wang, *A general strategy for numerical approximations of non-equilibrium models—part I: thermodynamical systems*, Int. J. Numer. Anal. Model. **15** (2018), no. 6, 884–918. MR3813735

[65] J. Zhu, L. Q. Chen, J. Shen, and V. Tikare. Coarsening kinetics from a variable mobility Cahn-Hilliard equation - application of semi-implicit Fourier spectral method. *Phys. Review E.*, 60:3564–3572, 1999.

[66] Q. Zhuang and J. Shen, *Efficient SAV approach for imaginary time gradient flows with applications to one- and multi-component Bose-Einstein condensates*, J. Comput. Phys. **396** (2019), 72–88, DOI 10.1016/j.jcp.2019.06.043. MR3979103

DEPARTMENT OF MATHEMATICS, PURDUE UNIVERSITY, WEST LAFAYETTE, INDIANA 47906
Email address: shen@math.purdue.edu

DEPARTMENT OF MATHEMATICS, UNIVERSITY OF SOUTH CAROLINA, COLUMBIA, SOUTH CAROLINA 29208
Email address: xfyang@math.sc.edu